A NEURAL NETWORK APPROACH FOR THE PREDICTION OF GROUND VIBRATIONS INDUCED DUE TO BLASTING

A thesis submitted in partial fulfilment of the requirements for the degree of

Bachelor of Technology & Master of Technology
(Dual Degree)
in
Mining Engineering

By
SAMRESH KUMAR PRADHAN
711MN1145

Department of Mining Engineering
National Institute of Technology
Rourkela – 769008, INDIA
2015-16

A NEURAL NETWORK APPROACH FOR THE PREDICTION OF GROUND VIBRATIONS INDUCED DUE TO BLASTING

A thesis submitted in partial fulfilment of the requirements for the degree of

Bachelor of Technology & Master of Technology
(Dual Degree)
in
Mining Engineering

By
SAMRESH KUMAR PRADHAN
711MN1145

Under the Supervision of
Prof. Singam Jayanthu

Department of Mining Engineering
National Institute of Technology
Rourkela – 769008, INDIA
2015-16

National Institute of Technology
Rourkela

CERTIFICATE

This is to certify that the thesis entitled **"A neural network approach for the prediction of ground vibrations induced due to blasting"** submitted by **Mr. Samresh Kumar Pradhan** in partial fulfilment of the requirements for the award of Bachelor of Technology & Master of Technology Dual Degree in Mining Engineering at National Institute of Technology, Rourkela is an authentic work carried out by him under my supervision and guidance.

To the best of my knowledge, the matter embodied in the thesis has not been submitted to any other University/Institute for the award of any Degree or Diploma.

Date:

Prof. Singam Jayanthu
Senior Professor
Department of Mining Engineering
National Institute of Technology
Rourkela – 769008

National Institute of Technology
Rourkela

ACKNOWLEDGEMENT

I would like to express my deep appreciation to my project guide **Prof. Singam Jayanthu** who has always been a source of motivation to me for carrying out the project. His constant inspiration and ideas have helped me in shaping this project very well. I am thankful to him for giving me his valuable time despite of his busy schedule to help me complete my project.

A word of thanks goes to **Prof. M.K.Mishra**, Head of the Department (Mining Engineering) for allowing me to use the facilities available in the department beyond office hours and to all the Faculty members, Staff and Students of the Department of Mining Engineering who have helped me in carrying out this work.

I would also like to thank the management of **Indian Detonators Ltd Rourkela, Dunguri Limestone Mine ACC Bargarh and Balphimali Bauxite Mine UAIL** for allowing me to collect the PPV and Frequencies values of various blasts carried out in their mines.

And more importantly I would like to thank my family and friends for supporting me in every possible way while carrying out this project work.

Samresh Kumar Pradhan
Department of Mining Engineering
National Institute of Technology
Rourkela – 769008, INDIA

ABSTRACT

This project presents the application of neural networks as well as statistical techniques for prediction of ground vibration by major influencing parameters of blast design. The predictions by artificial neural network (ANN) is compared with the predictions of conventional statistical relation. Ground vibrations and frequency induced due to blasting were monitored at Indian Detonators Limited Rourkela (IDL), Balphimali Bauxite mine (UAIL) and Dunguri Limestone mine (ACC). The neural network was trained by the data sets recorded at the various mine sites. From the analysis it was observed that the correlation coefficient determined for PPV and frequency by ANN was higher than the correlation coefficient of statistical analysis. The correlation coefficient determined for PPV and frequency by ANN for Balphimali Bauxite mine (UAIL) was 0.9563 and 0.9721 respectively and correlation coefficient determined for PPV and frequency by ANN for IDL was 0.9053 and 0.9136 while correlation coefficient determined for PPV and frequency by ANN for Dunguri Limestone mine (ACC) was 0.9322 and 0.9301. The difference in correlation coefficient of PPV and frequency in different mines is due to different number of input parameters for the neural network and number of datasets used for the training of network. The number of datasets and input parameters were more for Balphimali Bauxite mine (UAIL), thus it showed higher correlation coefficient between the recorded and predicted data by ANN than other mines.

CONTENTS

SL. NO.	PARTICULARS	PAGE NO.
	ABSTRACT	i
	LIST OF TABLES	iv
	LIST OF FIGURES	v
	CHAPTER-1 INTRODUCTION	
1	INTRODUCTION	2
1.1	OBJECTIVE	3
1.2	PLAN OF WORK	3
	CHAPTER-2 LITERATURE REVIEW	
2	LITERATURE REVIEW	5
2.1	IMPORTANT FINDINGS OF WORK DONE BY OTHERS ON PREDICTION OF GROUND VIBRATIONS AND FREQUENCY BY THE USE OF NEURAL NETWORKS	16
	CHAPTER-3 FUNDAMENTALS OF NEURAL NETWORKS	
3.1	ARTIFICIAL NEURONS	19
3.2	ARTIFICIAL NEURAL NETWORK	21
3.3	BACKPROPAGATION NEURAL NETWORK	22
3.4	ERROR BACK-PROPAGATION ALGORITHM	22
3.5	NEURAL NETWORK DESIGN AND ARCHITECTURE	28
3.6	TRAINING PARAMETERS	29
3.7	DATA SCALING AND REPRESENTATION AND WEIGHT INITIALIZATION	29
	CHAPTER-4 DETAILS OF BLAST SITES	
4.1	DUNGRI LIMESTONE MINE	31
4.1.1	BLASTING PRACTICES AT THE MINE	32
4.1.2	OBSERVATIONS RECORDED AT DUNGURI LIMESTONE MINE	34
4.2	IDL EXPLOSIVES LIMITED	35

4.2.1	DETAILS OF BLASTING FOR THE PURPOSE OF METAL CLADDING	35
4.2.2	OBSERVATIONS RECORDED AT IDL EXPLOSIVES LTD. ROURKELA	36
4.3	BAPHLIMALI BAUXITE MINE (UAIL)	36
4.3.1	BLASTING PRACTICES AT THE MINE	36
4.3.2	MINING METHOD	37
4.3.3	OBSERVATIONS RECORDED AT UAIL	40
	CHAPTER-5 **RESULTS AND COMPARISON**	
5.1	DUNGRI LIMESTONE MINE, ACC	42
5.2	IDL	50
5.3	UAIL	58
5.4	OVERALL ANALYSIS	66
5.5	PPV PREDICTED FOR VARIOUS MINES	67
	CHAPTER-6 **CONCLUSIONS AND SCOPE FOR FUTURE WORK**	
6.1	CONCLUSIONS	71
6.2	SCOPE FOR FUTURE WORK	72
	REFERENCES	

LIST OF TABLES

Sl. No.	Particulars	Page No.
1	Damage criteria vis-à-vis Buildings / Structures belonging to the owner	15
2	Damage criteria vis-à-vis Buildings / Structures NOT belonging to the owner	15
3	Important Findings of work done by others on prediction of ground vibrations and frequency by the use of neural networks	16
4	Observations recorded at Dunguri Limestone Mine	34
5	Observations recorded at IDL explosives Ltd. Rourkela	36
6	Observations recorded at UAIL	40
7	Error calculation of PPV of ACC predicted by ANN & MVRA	42
8	Error calculation of Frequency of ACC predicted by ANN & MVRA	46
9	Error calculation of PPV of IDL predicted by ANN & MVRA	50
10	Error calculation of Frequency of IDL predicted by ANN & MVRA	54
11	Error calculation of PPV of UAIL predicted by ANN & MVRA	58
12	Error calculation of Frequency of UAIL predicted by ANN & MVRA	62
13	Correlation coefficient between the recorded and predicted data at various mines	66
14	Predicted PPV (mm/sec) by ANN at different Distances from the source of blast at ACC	67
15	Predicted PPV (mm/sec) by ANN at different Distances from the source of blast at IDL	68
16	Predicted PPV (mm/sec) by ANN at different Distances from the source of blast at UAIL	69

LIST OF FIGURES

Sl. No.	Particulars	Page No.
1	Flowchart of the plan of work	3
2	Pictorial representation of the various zones and the Phenomenon of reflection of waves	7
3	Characteristic of P-Wave in a solid medium	8
4	Characteristic of S-Wave in a solid medium	8
5	Characteristic of Rayleigh wave in a solid medium	9
6	Vibration Components	9
7	Schematic representation of an artificial neuron	20
8	Activation function for neurons	20
9	Scheme of an artificial neural network	21
10	Graph of jagged error surface of error vs. weights	28
11	Dunguri limestone mine of ACC Ltd and nearby residential areas	31
12	General blasting pattern followed at Dunguri mine, ACC	32
13	General charging pattern followed at Dunguri mine, ACC	33
14	Charging of blast hole with Supergel explosive at Dunguri mine, ACC	34
15	Preparation of blast with powder explosive for metal cladding at IDL –Explosives Limited-Rourkela	35
16	Mine Plan showing location of site of experimental blast at UAIL	38
17	Charging of blast hole with SME	39
18	Charging of SME in the blast hole	39
19	Regression analysis between recorded and predicted PPV of ACC by ANN	43
20	Regression analysis between recorded and predicted PPV of ACC by MVRA	43
21	Line graph comparison between recorded and predicted PPV of ACC by ANN	44
22	Line graph comparison between recorded and predicted PPV of ACC by MVRA	44
23	Line graph comparison between recorded and predicted PPV of ACC by ANN & MVRA	45

24	Bar graph comparison between recorded and predicted PPV of ACC by ANN & MVRA	45
25	Regression analysis between recorded and predicted Frequency of ACC by ANN	47
26	Regression analysis between recorded and predicted Frequency of ACC by MVRA	47
27	Line graph comparison between recorded and predicted Frequency of ACC by ANN	48
28	Line graph comparison between recorded and predicted Frequency of ACC by MVRA	48
29	Line graph comparison between recorded and predicted Frequency of ACC by ANN & MVRA	49
30	Bar graph comparison between recorded and predicted Frequency of ACC by ANN & MVRA	49
31	Regression analysis between recorded and predicted PPV of IDL by ANN	51
32	Regression analysis between recorded and predicted PPV of IDL by MVRA	51
33	Line graph comparison between recorded and predicted PPV of IDL by ANN	52
34	Line graph comparison between recorded and predicted PPV of IDL by MVRA	52
35	Line graph comparison between recorded and predicted PPV of IDL by ANN & MVRA	53
36	Bar graph comparison between recorded and predicted PPV of IDL by ANN & MVRA	53
37	Regression analysis between recorded and predicted Frequency of IDL by ANN	55
38	Regression analysis between recorded and predicted Frequency of IDL by MVRA	55
39	Line graph comparison between recorded and predicted Frequency of IDL by ANN	56
40	Line graph comparison between recorded and predicted Frequency of IDL by MVRA	56
41	Line graph comparison between recorded and predicted Frequency of IDL by ANN & MVRA	57
42	Bar graph comparison between recorded and predicted Frequency of IDL by ANN & MVRA	57

43	Regression analysis between recorded and predicted PPV of UAIL by ANN	59
44	Regression analysis between recorded and predicted PPV of UAIL by MVRA	59
45	Line graph comparison between recorded and predicted PPV of UAIL by ANN	60
46	Line graph comparison between recorded and predicted PPV of UAIL by ANN	60
47	Line graph comparison between recorded and predicted PPV of UAIL by ANN & MVRA	61
48	Bar graph comparison between recorded and predicted PPV of UAIL by ANN & MVRA	61
49	Regression analysis between recorded and predicted Frequency of UAIL by ANN	63
50	Regression analysis between recorded and predicted Frequency of UAIL by MVRA	64
51	Line graph comparison between recorded and predicted Frequency of UAIL by ANN	64
52	Line graph comparison between recorded and predicted Frequency of UAIL by MVRA	65
53	Line graph comparison between recorded and predicted Frequency of UAIL by ANN & MVRA	65
54	Bar graph comparison between recorded and predicted Frequency of UAIL by ANN & MVRA	66

CHAPTER-1
INTRODUCTION

INTRODUCTION

The primary objective of blasting in mining is to break and move the rock. Whilst most blasts arguably achieve this objective reasonably efficiently, some of the energy applied to the rock by the detonating blast is inevitably converted into non-productive "waste" energy in the form of ground vibration and air blast. This energy leaves the vicinity of the blast and can travel a significant distance (as much as thousands of meters) before finally dissipating to negligible levels. In the meantime, it can cause significant damage to rock structures and buildings, and disturbance to human occupants.

Ground vibrations are an integral part of the process of rock blasting and consequently they are unavoidable. With the general trend toward large blasts in mining and constructions projects, vibration problems and complaints have also increased. Consequently, lawsuit cases have developed between the mining industry and the general public at an accelerating rate. Complaints ranges from human disturbance to outright demolition of a residential structure, and although some of these claims are exaggerated, other legitimate. In spite of the many varying damage criteria established in the past, it is difficult to completely isolate vibration damage from damage caused by natural setting of the building, inadequate construction, old ages, etc. Even if a valid "fool proof" damage criterion were established, the critical problem remains to eliminate or considerably reduce all complaints resulting from ground vibrations and air blast, regardless of what the prevailing legal vibration limits are within a community. Therefore, the effect of ground vibrations produced by blasting on building structures and human beings need to be predicted, monitored, and controlled by the blasting engineer as part of optimizing the job.

1.1 OBJECTIVES

To study the ground vibrations and frequency caused due to blasting and prediction of safe explosive amount and steps to be taken to reduce the adverse effects of blasting i.e. to reduce the Peak particle velocity (PPV) by the use of neural networks. Figure 1 shows the plan of work.

1.2 PLAN OF WORK

1) PPV and Frequency monitoring at Balphimali Bauxite Mine (UAIL), Indian Detonators Ltd. and Dunguri Limestone Mine (ACC).
2) Use of ANN and statistical techniques to predict PPV and Frequency.
3) Comparison of results obtained from ANN and statistical methods.

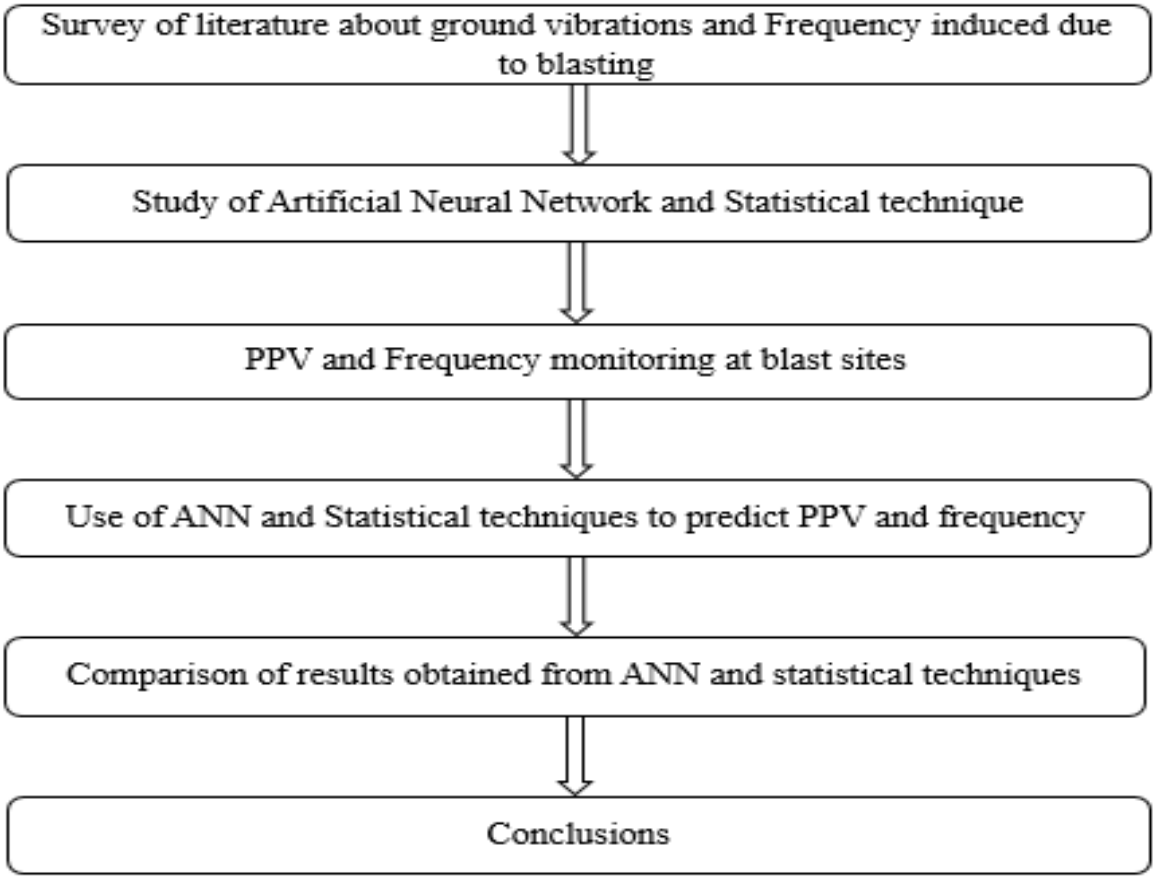

Fig 1: Flowchart of the plan of work

CHAPTER-2
LITERATURE REVIEW

LITERATURE REVIEW

Explosive energy produces the following effects:

- Rock shattering and displacement.
- Ground vibration.
- Air vibration.

The energy contained in explosives used in mine blastholes is designed to break and displace rock and the more energy available which can be utilised for that purpose, the more efficient the blast. However, some of the energy cannot be utilised in breaking rock and creates vibration in the surrounding rock and air. As a general principle, both air and ground vibration increase with increasing charge (explosive) mass and reduce with increasing distance.

Ground Vibration

The movement of any particle in the ground can be described in three ways; displacement, velocity and acceleration. Velocity transducers (geophones) produce a voltage which is proportional the velocity of movement, and can be easily measured and recorded. They are robust and relatively inexpensive and so are most frequently used for monitoring. It has been shown in many studies, most notably by USBM that it is velocity which is most closely related to the onset of damage, and so it is velocity which is almost always measured. If necessary, the velocity recording can be converted to obtain displacement or acceleration. Each trace has a point where the velocity is a maximum (+ve or -ve) and this is known as the Peak Particle Velocity (or PPV) which has units of mm/s. Geophones are only able to respond to vibration in one dimension and so to capture the complete signal it is necessary to have three geophones arranged orthogonally (at right angles). One will always be vertical and the other two will be horizontal, but the horizontal geophones can either be aligned with the cardinal points of the compass or they can be arranged with reference to the blast position. In the latter case, one geophone would be set along the line from blast to monitor (this is known as the longitudinal or radial) so that the other would be perpendicular to this line (this is known as the transverse).

Generation of blast vibration

When an explosive charge detonates, intense dynamic waves are set around the blast hole, due to sudden acceleration of the rock mass. The energy liberated by the explosive is transmitted to the rock mass as strain energy. The transmission of the energy takes place in the form of the waves. The energy carried by these waves crushes the rock, which is the immediate vicinity of the hole, to a fine powder. The region in which this takes place is called shock zone. The radius of this zone is nearly two times the radius of the hole. Beyond the shock zone, the energy of the waves gets attenuated to some degree which causes the radial cracking of the rock mass. The gas generated as a result of detonation enters into these cracks and displaces the rock further apart causing its fragmentation. The region in which this phenomenon takes place is called transition zone. The radius of this zone is twenty to fifty times the radius of the hole. As a result of further attenuation taking place in the transition zone, the waves although cause generation of the cracks to a lesser extent but they are not in a position to cause the permanent deformation in the rock mass located outside the transition zone. If these attenuated waves are not reflected from a free face, then they may cause vibrations in the rock. However, if a free face is available, the waves reflected from a free face cause further breakage in the rock mass under the influence of the dynamic tensile stress. Fig 3 is a pictorial representation of the various zones described above and explains the phenomenon of reflection of waves.

Wave forms of blast vibration

Ground vibration radiates outwards from the blast site and gradually reduces in magnitude, in the same manner as ripples behave when a stone is thrown into a pool of water, schematically shown below. The motion of the wave can be defined by taking measurements of a float on the surface of the water. With suitable instruments the displacement or amplitude, velocity, acceleration and wave length of the waves can be measured. Figure 2 shows the pictorial representation of the various zones and the phenomenon of reflection of waves

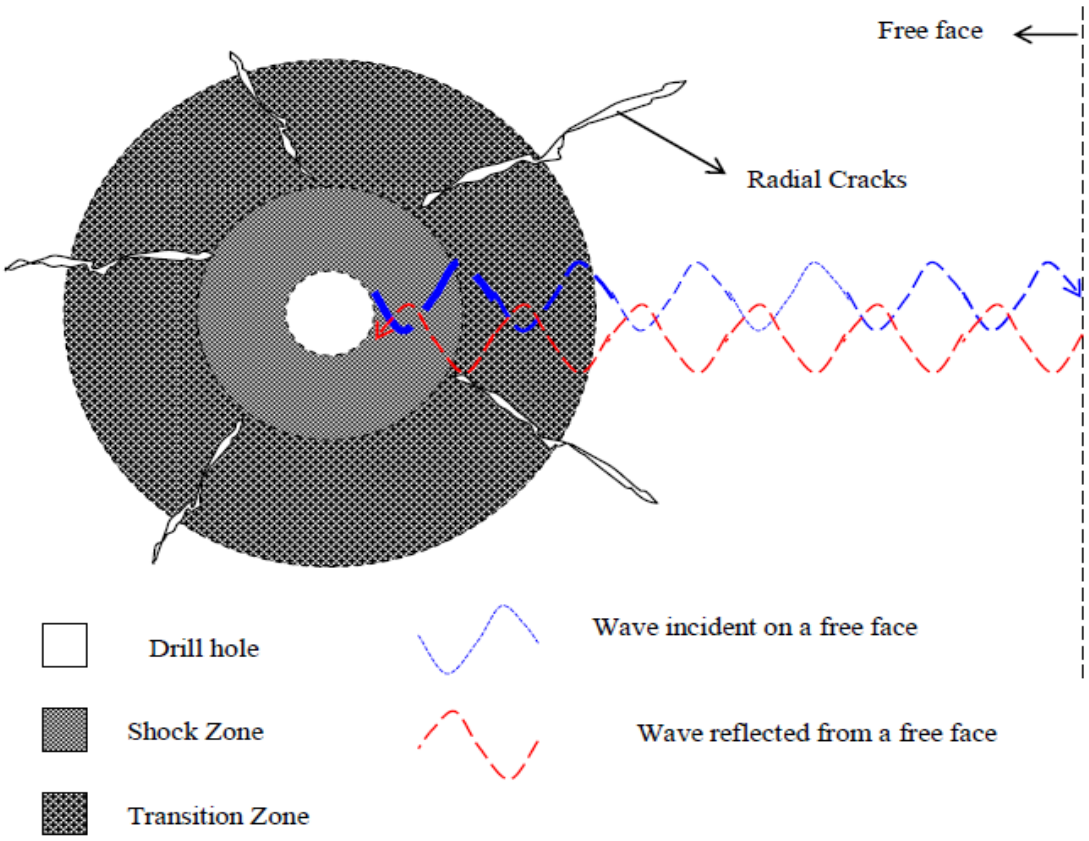

Fig 2: Pictorial representation of the various zones and the Phenomenon of reflection of waves

The ground vibration wave motion consists of different kinds of waves:

- Compression (or P) waves.
- Shear (or S or secondary) waves.
- Rayleigh (or R) waves.

P-wave

The Compression or "P" wave is the fastest wave through the ground. The simplest illustration of the motion of the particles within the "P" wave is to consider a long steel rod struck on the end. The particles of the rod move to and fro as the compressive pulse travels along the rod, i.e. the

particles in the wave move in the same direction as the propagation of the wave. The "P" wave moves radially from the blasthole as shown in figure 3 in all directions at velocities characteristic of the material being travelled through (approximately 2200 m/s).

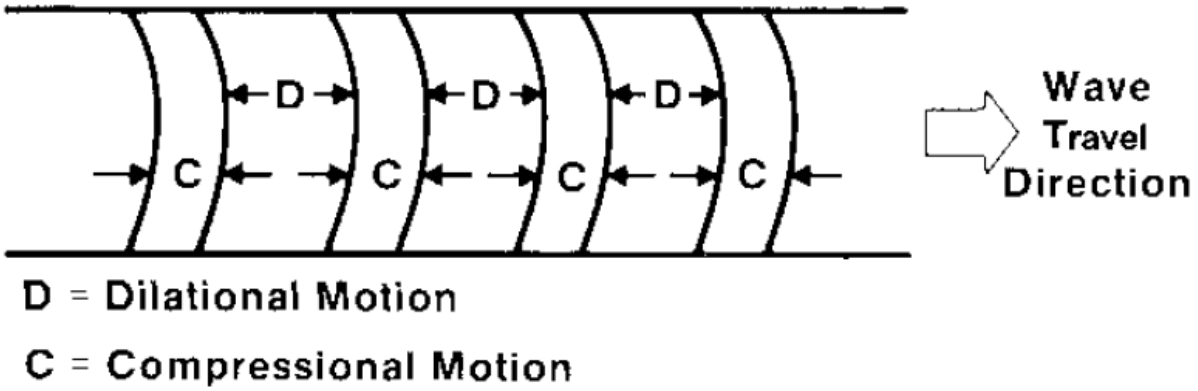

Fig 3: Characteristic of P-Wave in a solid medium

S-wave

The Shear or "**S**" wave travels at approximately 1200 m/s (50% to 60% of the velocity of the "P" wave). The motion of the particles within the wave can be illustrated by shaking a rope at one end as shown in Figure 4. The wave travels along the rope, but the particles within the wave move at right angles to the direction of motion of the wave. The "P" waves and "S" waves are sometimes referred to as ―body waves because they travel through the body of the rock in three dimensions.

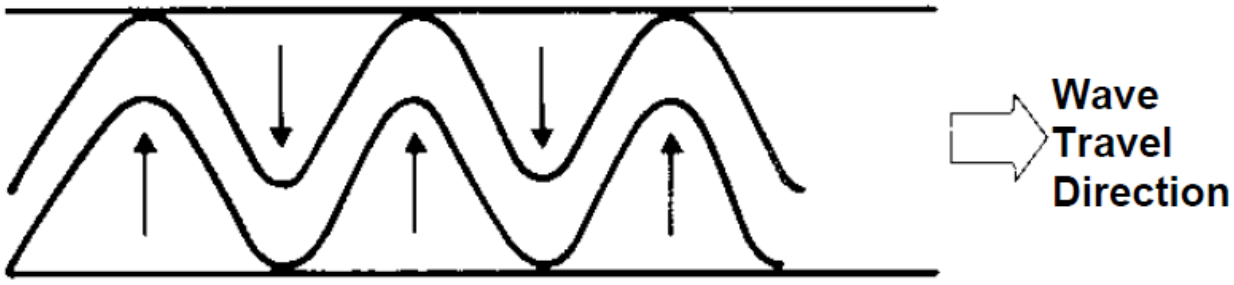

Fig 4: Characteristic of S-Wave in a solid medium

R-wave

The R-wave propagates more slowly than the P-wave and S-wave and the particles move elliptically in the vertical plane and in the same direction as the propagation. Unlike the body wave's unidirectional particle motions, Rayleigh surface wave particle motion is two dimensional.

These waves are similar to those produced by dropping a stone into a pool of water. As the water wave passes a piece of cork, the motion of the cork on water is described by a forward circle. Whereas, in rock a particle will follow a retrograde elliptical path, with the ratio of horizontal to vertical displacements equal to 0.7.

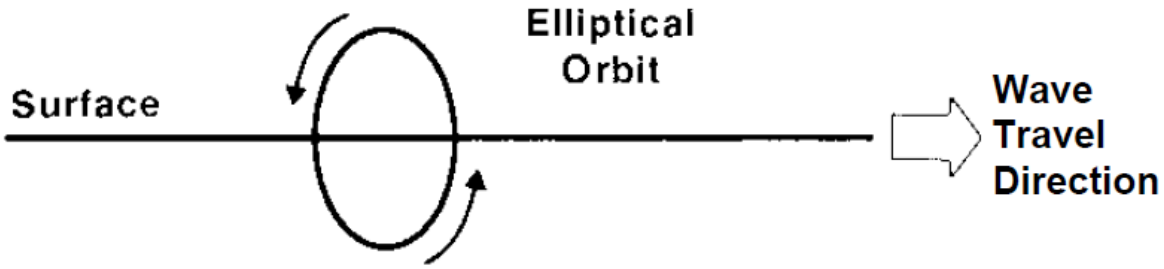

Fig 5: Characteristic of Rayleigh wave in a solid medium

To describe the motions completely, three perpendicular components of motion must be measured; the longitudinal, L, is usually oriented along a horizontal radius to the explosion. It follows, then, that the other two perpendicular components will be vertical, V, and transverse, T, to the radial direction, as shown in Figure 5.

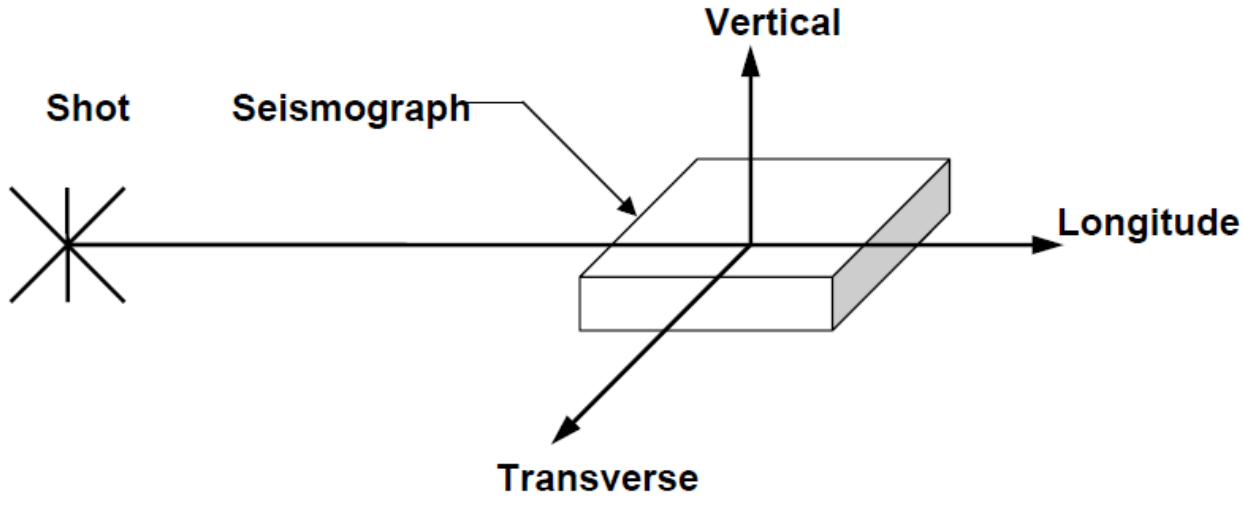

Figure 6: Vibration Components

None of these vibration components as shown in Figure 6, which are normal to each other, always dominates in blasting and the peak component varies with each blasting site. The peak occurs in different times and at different frequencies. The difference between the three components results from the presence of the different wave types in the blast vibration wave trains.

Peak Component and True Vector Sum

The variation of motion with each component has led to difficulty in determining which component is the most important. Is it the component with the greatest amplitude, or the peak vector sum of the components? Assume that we have the peak component of 0.9 of velocity unit recorded in longitudinal direction at time 1, and the vertical and the transverse components at the same time are 0.25 and 0.25, respectively. The true vector sum of all the components at time 1 is

$$(L^2 + V^2 + T^2)^{0.5} = (0.9^2 + 0.25^2 + 0.25^2)^{0.5}$$
$$= 0.96 \text{ unit}$$

There may be another time when the peak true vector sum will be larger than that at the peak component and several should be checked. However, it usually occurs at the same time as the largest component peak. Peak motions should always be reported as either peak component or the peak true vector sum.

Another measure, the maximum vector sum, is frequently reported but is conservative and not directly related to a maximum velocity at a particular time. The maximum vector sum is calculated as shown in the above equation also; however, the maximum of each component is used regardless of the time when it occurs. Thus, for the same record in the example above if the peak of the vertical and transverse components are both 0.75 and occur at different time than time 1, then, the maximum vector sum is

$$(0.9^2 + 0.75^2 + 0.75^2)^{0.5} = 1.4 \text{ unit}$$

In general, the empirical observations of cracking have been made with single-component peaks; therefore, use of the maximum vector sum provides a large unaccounted safety factor. As a result of that, peak particle velocity, which is the maximum particle velocity among the radial, vertical, and transverse components recorded form the same blast event, should be taken into account instead of peak vector sum.

Frequency Properties and Durations

The frequency of ground vibration can be defined as the number of cycles executed per unit time (second). Mathematically, it can be expressed as follows:

$$F = 1/T$$

Where F is the frequency and its unit is Hertz (Hz), and T is the time in seconds required for a complete oscillation. The amplitude (A) of ground vibration is defined as a time varying and kinematical vibration quantity of displacement, velocity or acceleration. They all have instantaneous values at any instant together with the peak or maximum at some specific moments for any vibration record. The amplitude, frequencies, and durations of the ground vibrations change as they propagate, because of (a) interaction with various geologic media and structural interfaces, (b) spreading out the wave-train through dispersion, and/or (c) absorption, which is greater for the higher frequencies. Therefore, the vibration frequency and consequently the velocity, displacement and acceleration amplitudes depend strongly on the propagating media. For instance, thick soil overburden as well as long absolute distance creates long-duration, low-frequency wave trains. This increases the responses and damage potential of nearby structures. The 1980 USBM's report indicates that frequencies below 10 Hz produce large ground displacement and high levels of strain, anvd also couple very efficiently into structures where typical resonant frequencies are 4 to 12 Hz for the corner or racking motions. It is also concluded that damage potentials for low-frequency blasts (<40 Hz) are considerably higher than those for high-frequency (>40Hz).

Parameters influencing propagation and intensity of ground vibrations

The parameters, which exhibit control on the amplitude, frequency and duration of the ground vibration, are divided in two groups as follows:

a. Non-controllable Parameters

b. Controllable Parameters

The non-controllable parameters are those, over which the Blasting Engineer does not have any control. The local geology, rock characteristics and distances of the structures from blast site is non-controllable parameters. However, the control on the ground vibrations can be established with the help of controllable parameters. The same have been reproduced below:

1. Charge Weight
2. Delay Interval
3. Type of Explosive
4. Direction of blast propagation

5. Burden, Spacing and Specific charge
6. Coupling
7. Confinement
8. Spatial Distribution of Charges

Reduction of ground vibrations

To protect a structure, it is necessary to minimize the ground vibrations from the blast. The acceptable techniques for reduction and control of vibrations are:

a. Reduce the charge per delay: This is the most important measure for the purpose. Charge per delay can be controlled by:

i. Reducing the hole depth.
ii. Using small diameter holes
iii. Delayed initiation of deck charges in the blast holes
iv. Using more numbers of delay detonators series
v. Using sequential blasting machine

b. Reduce explosive confinement by:

i. Reducing excessive burden and spacing
ii. Removing buffers in front of the holes
iii. Reducing stemming but not to the degree of increasing air-blast and fly rock
iv. Reducing sub-grade drilling
v. Allowing at least one free face
vi. Using decoupled charges
vii. Drilling holes parallel to the bench face
viii. Accuracy in drilling

c. Limit the explosive confinement to bedrock if the overburden can be excavated by other means.

d. Square patterns produce more vibrations

e. Limit frequency of blasting

f. Time the blasts with high ambient noise levels

g. Use controlled blasting techniques

h. Use a low VOD and low density explosive

Structure Response to Blast Excitation

Blasting can cause significant vibrations within structures even in cases where the distance between a blast and the structure is large. High levels of vibration within structures are caused by a close match between the ground vibration frequency and the fundamental resonant frequency of the structure or some structural elements

Structure Components and Ground Vibration Parameters

Structures consist of many components, and two of most important are walls and superstructural skeletons. Superstructure response, measured at a corner, is associated with the shearing and torsional distortion of the frame, while the wall response, which measured in the middle of the wall, is associated with bending of that particular wall. The wall and superstructure continue to vibration freely after the passage of the ground motion, according to Dowding (1985). He also indicated that the wall motion tend to be larger in amplitude than the superstructure motions and tend to occur at higher frequencies during free vibration than those of the superstructure. Detailed studies (Dowding et al., 1980; Medearis, 1976) have shown that the natural frequencies of walls range from 12 to 20 Hz and those of superstructures from 5 to 10 Hz.

The response of any structure to vibration can be calculated if its natural frequency and damping are known or can be estimated. The fundamental natural frequency Fd of the superstructure of any tall building can be estimated from compilations of work in earthquake engineering (Newmark and Hall, 1982):

$$F_d = 1 / 0.1*N$$

where, N is the number of the stories. Substitution of 1 and 2 for residential structures for N yields Fd values that can be compared favorably with results of actual measurements. Damping β is a function of building construction and to some extent the intensity of vibration. Measurement reveals a wide range of damping for residential structure with an average of 5%. Excessive structural response has been separated into three categories arranged below in the order of declining severity and increasing distance of occurrence (Nothwood et al., 1963; Siskind et al., 1980). Beginning with effects that occur closest to the blast, the categories are listed here:

1. Major (Permanent Distortion). Resulting in serious weakening of the structure (e.g. large cracks or shifting of foundations or bearing walls, major settlement resulting in distortion or weakening of the superstructure, walls out of plump).
2. Minor (Displaced Cracks). Surficial, not affecting the strength of the structure (e.g. broken windows, loosened or fallen plaster), hairline cracks in masonry.
3. Threshold (Cosmetic Cracking). Opening of old cracks and formation of new plaster cracks, dislodging of loose objects (e.g. loose bricks in chimneys) (Dowding, 1992).

Resonation and Amplification Factor

The probability of damage in structures depends on the relationship between dominant frequency of the ground vibration and natural frequency of the structure. Most significant for blasting is that the principal frequencies of the ground motion almost always equal or exceed the gross structure natural frequencies of 4 to 10 Hz. In this case, structure resonates and it is shacked by amplified vibration a few seconds. People may still perceive and are concerned about this situation. While structure resonates, it may not be damaged but people may still complain even if particle velocity is much below the limiting vibration value. However, the damages within the structures are caused when structure resonates at a particle velocity exceeding vibration limit. Although amplitude of the exciting wave traveling in the ground is not sufficient to cause damage to structure, structure may be damaged due to amplification during resonation. Amplification is defined as the increase in the amplitude measured in the structure with respect to ground amplitude due to the transfer of the exciting wave on the ground to the structure. The ratio of amplitude of the structure to ground amplitude is called as amplification factor.

Damage criteria:

The damage criteria was proposed by many organizations including USBM, DGMS, Indian Standards etc based on the Permissible PPV in mm/s and Frequency of the ground vibrations for various types of structures. The criteria based on the Permissible PPV in mm/s and Frequency of the ground vibrations for various types of structures as per DGMS (1997) as presented below in Table 1 and 2 is followed for the present investigations to estimate safe charge per delay to limit the ground vibrations within safe limit of 5 mm/sec as the frequency was within the limits of 8 to 25 for the present observations (considering the structures as sensitive and not belonging to the residential areas).

Table 1: Damage criteria vis-à-vis Buildings / Structures belonging to the owner

Type of Structure	Dominant Excitation Frequency		
	<8 Hz	8 to 25 Hz	> 25 Hz
a) Domestic Houses	10	15	25
b) Industrial Building	15	25	50
c) Sensitive Structure	2	5	10

Table 2: Damage criteria vis-à-vis Buildings / Structures NOT belonging to the owner

Type of Structure	Dominant Excitation Frequency		
	<8 Hz	8 to 25 Hz	> 25 Hz
a) Domestic Houses	10	15	25
b) Industrial Building	15	25	50

Distinction of blast-induced cracking from natural cracking

Control of blast-induced transient effects to prevent threshold or cosmetic cracking reduces blast-induced displacement or strains in structures to below that caused by every day activities and change in the weather (Stagg et al., 1984; Dowding, 1988). The blast induced threshold cracks can be scientifically observed only with visual inspection immediately before and after each blast. However, the multiple origins of cracks should be taken into consideration. Several institutional references (Anon, 1977; Anon, 1956; Thoenen and Windes, 1942) summarized that cracks basically are found to be caused by the following non-blast factors:

1- Differential thermal expansion.

2- Structural overloading.

3- Chemical change in mortar, bricks, plaster, and stucco.

4- Shrinking and swelling of wood.

5- Fatigue and aging of wall coverings.

6- Differential foundation settlement.

2.1 Important Findings of work done by others on prediction of ground vibrations and frequency by the use of neural networks

Table 3: Important Findings of work done by others on prediction of ground vibrations and frequency by the use of neural networks

Serial No.	Year	Author	Title	Important Findings
1	2010	P K Singh	Standardization of blast vibration damage threshold for the safety of residential structures in mining areas	Artificial neural network and fuzzy logic used to predict the safe explosive amount.
2	2009	Marathan Silitonga	Prediction of ground vibrations due to blasting	The potential of variations in vibration intensity due to blast constriction and its implication in vibration control.

3	2009	Roy Fitzgerald Nicholson	Determination of Blast Vibrations using PPV	A understanding of ground vibrations from blast and its effect on structures.
4	2009	Manoj Khandelwal, T.N. Singh	Evaluation of blast-induced ground vibration predictors	Neural network approach for appropriate prediction of PPV to protect surrounding environment and structures
5	2009	Mohamed	Use of ANN to predict blast induced vibrations	Author observed that the ANN model with two-input parameters provides better results than the model with one input parameter. That is to say, increase in the number of input variables results in increasing the ability of ANN to learn and to predict more precisely.
6	2008	Tang	Prediction of the peak velocity of blast vibration	Tang has adopted the back-propagation neural network model to predict the peak velocity of blast vibration
7	2008	M. Monjezi	A model to predict blast-induced ground vibration using artificial neural network (ANN) in the Siahbisheh project, Iran	To construct the model on maximum charge per delay, distance from blasting face to the monitoring point using ANN model.

CHAPTER-3
FUNDAMENTALS OF NEURAL NETWORKS

FUNDAMENTALS OF NEURAL NETWORKS

In 1956 the Rockefeller Foundation sponsored a conference at Dartmouth College that had as its scope:

The potential use of computers and simulation in every aspect of learning and any other feature of intelligence. It was at this conference that the term "artificial intelligence" came into common use.

Artificial intelligence can be broadly defined as:

Computer processes that attempt to emulate the human thought processes that are associated with activities that required the use of intelligence.

Neural networks technique recently has been included in this definition, so it can be accepted as a legitimate field of artificial intelligence (Tsoukalas and Uhrig, 1996).

3.1 Artificial Neurons

An artificial neuron is a model whose components have direct analogs to components of an actual neuron. Figure 7 shows the schematic representation of an artificial neuron. This artificial neuron was first presented by McCulloch and Pitts in 1943. The input signals are represented by *x0, x1, x2…, xn.* These signals are continuous variables, not the discrete electrical pulses that occur in the brain. Each of these inputs is modified by a *weight* (sometimes called the *synaptic weight)* whose function is analogous to that of the synaptic junction in a biological neuron. These weights can be either positive or negative, corresponding to acceleration or inhibition of the flow of electrical signals.

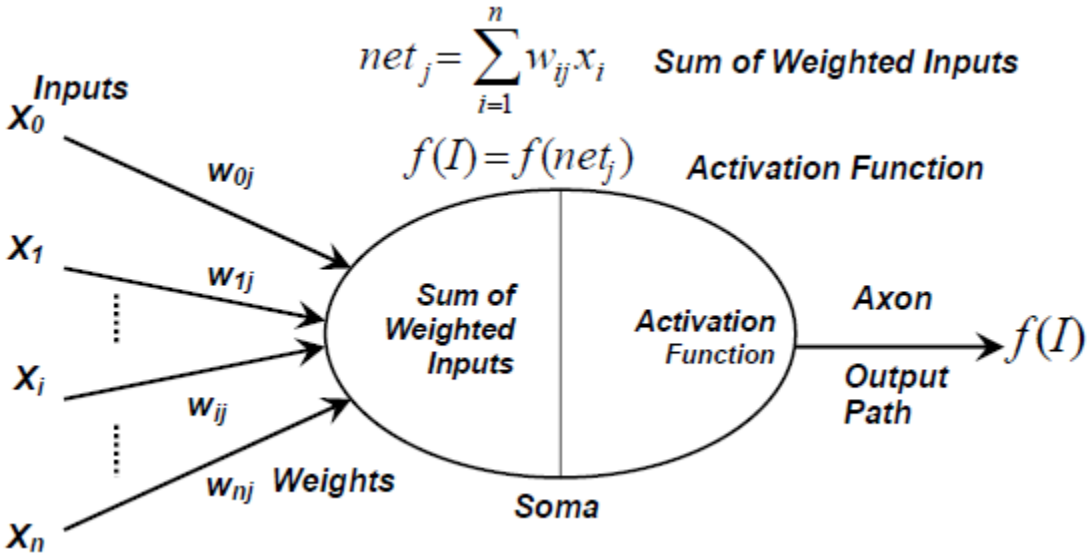

Fig 7: Schematic representation of an artificial neuron (Saha, 2003)

This processing element consists of two parts. The first part simply aggregates (sums) the weighted inputs resulting in a quantity,

$$I = \left(\sum_{i=1}^{n} w_{ij} x_i \right);$$

the second part is effectively a nonlinear filter, usually called the *activation function*, through which the combined signal flows (Tsoukalas and Uhrig, 1996). More commonly, the activation function is a continuous function that varies gradually between two asymptotic values, typically 0 and 1 or –1and +1, called the *sigmoidal function*. The most widely used activation function is the logistic function, which is shown in Figure 8 and represented by the equation.

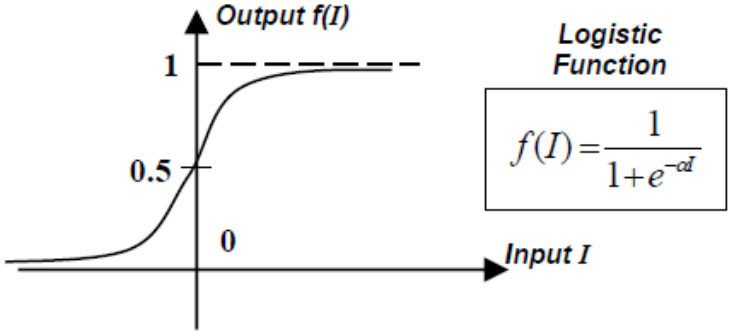

Fig 8: Activation function for neurons (Saha, 2003)

$$f(I) = \frac{1}{1 + e^{-\alpha I}}$$

Where α is a coefficient that adjusts the abruptness of this function as it changes between the two asymptotic values.

3.2 Artificial Neural Network

An artificial neural network can be defined as:

A data processing system consisting of a large number of simple, highly interconnected processing elements (artificial neurons) in an architecture inspired by the structure of the cerebral cortex of the brain (Tsoukalas and Uhrig, 1996).

These processing elements are usually organized into a sequence of layers or slabs with full or random connections between the layers. This arrangement is shown in Figure 9, where the input layer is a buffer that presents data to the network.

The following layer(s) is called the hidden layer(s) because it usually has no connection to the outside world. The output layer is the following layer in the network, which presents the output response to a given input. Typically, the input, hidden, and output layers are designated the *i*th, *j*th, and *k*th layers, respectively.

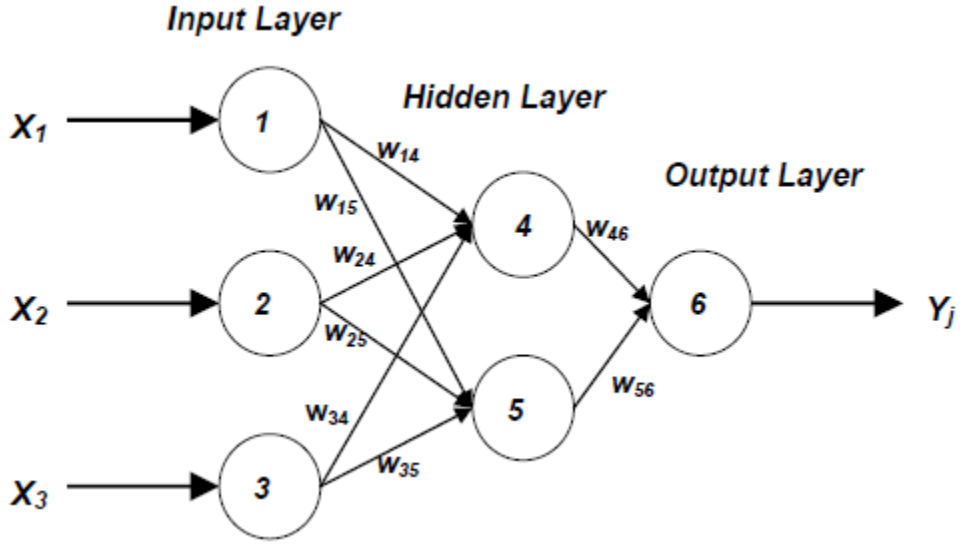

Fig 9: Scheme of an artificial neural network (Saha, 2003)

Typical neural network is "fully connected," which means that there is a connection between each of the neurons in any given layer with each of the neurons in the next layer as shown in Figure 9. When there are no lateral connections between neurons in a given layer and none back to previous layers, the network is said to be a feedforward network (Tsoukalas and Uhrig, 1996). This network is said to be trained until the Least-mean-square (LMS) is minimized. The LMS is defined by the equation

$$E_p = \frac{1}{2}\sum_{j}^{N}(t_{pj} - o_{pj})^2$$

Where *tpj* and *opj* are the target and actual outputs for pattern *p* on node *j*, respectively.

3.3 Backpropagation Neural Network

Backpropagation is a systematic method for training multiple (three or more)- layer artificial neural networks. The clarification of this training algorithm by Rumelhart, Hinton, and Williams (1986) was the key step in making neural networks practical in many real-world situations. However, Rumelhart, Hinton, and Williams were not the first to develop the backpropagation algorithm. It was developed independently by Parker (1982) in 1982 and earlier by Werbos (1974) in 1974. Nevertheless, the backpropagation algorithm was critical to the advances in neural networks because of the limitations of the one-and two-layer networks discussed previously. Indeed, backpropagation played a critically important role in the resurgence of the neural network field in the mid-1980s. Today, it is estimated that 80% of all applications utilize this backpropagation algorithm in one form or another. In spite of its limitations, backpropagation has dramatically expanded the range of problems to which neural network can be applied, perhaps because it has a strong mathematical foundation (Tsoukalas and Uhrig, 1996).

3.4 Error Back-propagation Algorithm

Error back-propagation is a learning scheme in which the error is backpropagated and used to update the weights. The algorithm employs a gradient descent method that minimizes the error

between the desired and actual outputs calculated by the multilayer perceptron (Rumelhart and Hinton, 1986). Back-propagation and error adjustment continue until all examples from the training set are learnt within an acceptable overall error. The following is the scenario for the *pth* pattern in a feedforward network with hidden layers.

1. The *ith* node in the input layer holds a value of *xpi* for the *pth* pattern.
2. The net input to the *jth* node in the hidden layer for pattern *p* is

$$net_{pj} = \sum_{i}^{N} w_{ij} o_{pi}$$

Where *wij* is the weight from node *i* to node *j*. the output from each unit *j* is the threshold function, *fj,* which acts on the weighted sum. In this multilayer perceptron *fj* is the sigmoid function, defined as

$$f(net) = \frac{1}{(1+e^{-knet})}; (0 < f(net) < 1)$$

Where *k* is a positive constant that controls the spread of the function.

3. The output of the *ith* node in the hidden layer can also defined as

$$o_{pj} = f_j(net_{pj})$$

4. The net input to the *kth* node of the output layer is

$$net_k = \sum_{j} w_{kj} x_{pj}$$

Where *wkj* is the weight values between the *ith* hidden layer and the *kth* output layer node.

5. Output of the *kth* node of the output layer can also be defined as

$$o_{pk} = f_k(net_k)$$

6. If *Ep* is the error function for a pattern, *p*, that is proportional to the square of difference between the actual and desired outputs for all the patterns to be learnt

$$E_p = \frac{1}{2}\sum_{k}^{N}(t_{pk} - o_{pk})^2$$

Where *tpk* and *opk* are the target and actual outputs for pattern *p* on node *k*, respectively.

In more general setting, with more than one hidden layer, weight $w_{kj}^{(i+1,i)}$ denotes the weight assigned to the link from node *j* in the *ith* layer to node *k* in the *(i+1)th* layer, and x_{pj}^{i} denotes output of the *jth* node in the *ith* layer for the *pth* pattern (Mehrotra et. al., 1996). Now it is needed to discover *w*, the vector consisting of all weights in the network, such that the value of *Ep* is minimized. One way to minimize E is based on the gradient decent method. According to this method, the direction of weight change of w should be in the same direction as - *∂E/∂w*. To simplify the calculation of -*∂E/∂w,* the weight change in a single weight is examined. the value of *∂E/∂wkj* is calculated for each connection from the hidden layer to the output layer. Similarly, the value of *∂E/∂wji* is calculated for each connection from the input layer to the hidden layer. The connection weights are then changed by using the value so obtained; this method is also known as the *generalized delta rule*. In brief, the following two equations describe the suggested weight changes.

$$\Delta w_{kj} \propto \left(\frac{-\partial E}{\partial w_{kj}} \right)$$

$$\Delta w_{ji} \propto \left(\frac{-\partial E}{\partial w_{ji}} \right)$$

The derivative of *E* with respect to a weight *wkj* associated with the link from node *j* of the hidden layer to the *kth* node of the output layer is easier to calculate than for a weight *wji* connecting the *ith* node of the input layer to the *jth* node of the hidden layer. But both calculations use the same general idea–the chain rule of derivatives. The error depends on *wkj* only through *opk*, hence, for the calculations that follow, it is sufficient to restrict attention to the partial derivative of *E* with respect to *opk* and then differentiate *opk* with respect to *wkj*. From equation (2.14), the following equation is obtained

$$\frac{\partial E}{\partial o_{pk}} = -2(t_{pk} - o_{pk})$$

Since equation (2.12) represents the total input to a node *k* in the output layer, and equation () gives the output, *opk*, hence;

$$\frac{\partial o_{pk}}{\partial net_k} = S'(net_k)$$

and,

$$\frac{\partial net_k}{\partial w_{kj}} = x_j$$

Consequently, the chain rule is

$$\frac{\partial E}{\partial w_{kj}} = \frac{\partial E}{\partial o_{pk}} \frac{\partial o_{pk}}{\partial net_k} \frac{\partial net_k}{\partial w_{kj}}$$

Which gives

$$\frac{\partial E}{\partial w_{kj}} = -2(t_{pk} - o_{pk}) S'(net_k) x_j$$

Next, consider the derivative of *(∂E / ∂wji)*. The error *E* depends on *wji* through *netj*, also,

$o_{pk} = S(net_k), x_j = S(net_j)$

and

$net_j = \sum_i w_{ji} \times x_i$

Therefore, using the chain rule of derivatives, the following equation is

Obtained

$$\frac{\partial E}{\partial w_{ji}} = \sum_{k=1}^{K} \frac{\partial E}{\partial o_{pk}} \frac{\partial o_{pk}}{\partial net_k} \frac{\partial net_k}{\partial x_j} \frac{\partial x_j}{\partial net_j} \frac{\partial net}{\partial w_{ji}}$$

$$= \sum_{k=1}^{K} \left\{ -2(t_{pk} - o_{pk}) S'(net_k) w_{kj} S'(net_j) x_i \right\}$$

From equations 2.15 and 2.21, the weight changes at the outer layer of weights can be summarized as

$$\Delta w_{kj} = \eta \times \delta_k \times x_j$$

and from equation 2.13 and 2.24, weight changes at the inner layer of weights are

$$\Delta w_{ji} = \eta \times \mu_j \times x_i$$

Where η is an independent parameter known as the "learning rate," and its value ranges between 0 and 1, and

$$\delta_k = (t_{pk} - o_{pk}) S'(net_k)$$

And

$$\mu_j = (\sum_k \delta_k w_{kj}) S'(net_j)$$

Thus, similar equations determine the change in both layers of weights proportional to the product of the input to the weight in the forward direction (*xj* or *xi*) and a generalized error term (*δk or μj*).

- The value of *δk* is proportional to the amount of error *(tpk–opk)* multiplied by the derivative of the output node with respect to the net input to the output node.
- The value of *μj* is proportional to the amount of weighted error *Σk δk wkj* (using the previous layer's *δ* values) multiplied by the derivative of the output of the hidden node with respect to the net input of the hidden node.

The above analysis does not make any assumption about the node activation function except that it should be differentiable. For the sigmoid function

$$S(x) = \frac{1}{(1 + e^{-x})}$$

, the derivative $S'(x) = \partial S(x) / \partial x$ is equal to **= *S(x)(1 – S(x))***

Hence, if every node uses this node function, then

$$\delta_k = (t_{pk} - o_{pk}) o_{pk} (1 - o_{pk})$$

And

$$\mu_j = \sum_k \delta_k w_{kj} x_j (1 - x_j)$$

Thus, the weight updating for every individual weight *wij*, between the output layer and hidden layer, can be done using the following formula

$$w_{new} = w_{old} + \eta * (\delta_k * x_j)_{w_{old}}$$

and, for the weights between the hidden layer and the input layer, the following formula can be used

$$w_{new} = w_{old} + \eta * (\mu_j * x_j)_{w_{old}}$$

In brief, there are two phases of back-propagation algorithm;

1. Present input patterns, propagate activation through output to generate *opk* for each output unit. Then compare the output against the desired output, to calculate the error signals.
2. Pass error backwards through the network so as to recursively compute error signals, and use them to update weights of the previous layers.

However, back-propagation may lead the weights in a neural network to a local minimum of the mean-square-error (MSE), possibly substantially different from the global minimum that corresponds to the best choice of weights. This problem can be particularly bothersome if the "error surface" (plotting MSE against network weights) is highly uneven or jagged, Figure 10.

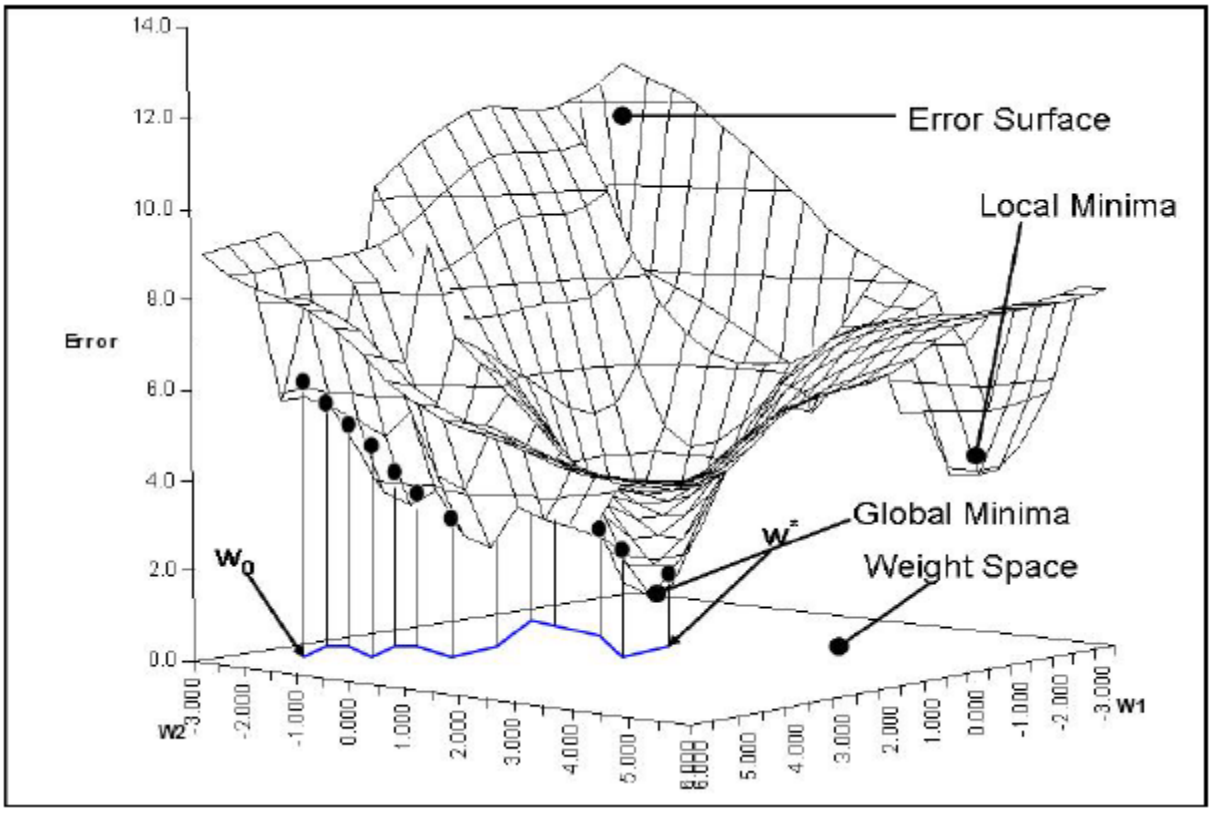

Fig 10: Graph of jagged error surface of error vs. weights (Saha, 2003)

To avoid getting stuck in the local minimum, another term can be added to the weight updation formula; this term is called the "*momentum*".

$$w_{n+1} = w_n + \eta^*(\delta_k * x_j)_{w_{(n)}} + \alpha^*(w_n - w_{n-1})$$

Where, α is the momentum coefficient and its value ranges between 0 and 1 (typically about 0.9).

3.5 Neural Network Design and Architecture

Many important issues, such as determining how large a neural network is required for a specific task, and how many nodes and layers should be included in the network design, are solved in practice by trial and error. For instance, with too few number of nodes, the network may not be powerful enough for a given learning task. With a large number of nodes (and connections), computation is too expansive. Neural learning is considered successful only if the model can perform well on test data on which the network has not been trained.

3.6 Training Parameters

The training parameters, the learning rate and the momentum (typical values between 0 and 1) have a significant effect on the training process. A large value of learning rate will lead to rapid learning but the weight may then oscillate, while low values imply slow learning and it takes long time to converge to global minima. A high value of a momentum coefficient allows one to choose higher value of learning rate. In fact, there is no clear consensus on any fixed strategy in choosing the proper values of the training parameters. However, in practice, the best choice can be achieved by trial and error, which leads to the minimum prediction error (Tsoukalas and Uhrig, 1996).

3.7 Data Scaling and Representation and Weight Initialization

Scaling has the advantage of mapping the desired range of a variable (with range between the minimum and maximum values) to the full "working" range of the network input and output. Scaling of the variable between 0.1 and 0.9 is often used to limit the amount of the sigmoid activation function used in the representation of the variables in order to avoid "network paralysis" in the training process. In addition to that, the data is represented randomly to the neural network for each training cycle, which means the data is fedforward to the network in different order for each epoch. This randomization of the input patterns helps in speeding up the training process and takes less time to converge to global minima. Moreover, training is generally commenced with randomly chosen weight values. Typically, the weight chosen are (between -1.0 and 1.0 or -0.5 to +0.5), since large weight magnitudes may drive the output of layer 1 nodes to saturation, requiring large amounts of training time to emerge from the saturated state (Mehrotra et. al., 1996).

CHAPTER-4
DETAILS OF BLAST SITES

DETAILS OF BLAST SITES

4.1 DUNGRI LIMESTONE MINE

The Dungri Limestone mine is situated in the Bargarh District of Odisha. The village Dungri is situated at a distance of 850 meter from the active mine. The Dungri Limestone mine has a longitude of **83°32'57.4"** and latitude of **21°41'24"** The Dungri area is situated in the rich mining belt of Bargarh. Limestone is a very essential raw material for the metallurgical industry as flux and in the manufacture of cement. Large deposits of limestone are located all over the area and are being worked out. The Dungri Limestone mine is an entity of ACC Limited (Formerly The Associated Cement Companies Limited). The ACC is one of the largest producers of cement in India. The company is the only cement company to get Super brand status in India. The Dungri lease is in the shape of a rectangle parallel to Mahanadi River with northern portion of the area widening out in the shape of a polygon. The Lease area is in the low lying portion of the valley between the Dechua hill range in the east and the Holsary hills in the west with the ground sloping gently from west to east. The Mahanadi flows further west of the Holsary hills. Figure 11 shows the Dunguri limestone mine of ACC Ltd and nearby residential areas

Fig 11: Dunguri limestone mine of ACC Ltd and nearby residential areas (Google Maps)

4.1.1 BLASTING PRACTICES AT THE MINE

The Dungri limestone mine is fully mechanized mine being operated by drill and blast method for primary breakage and rock breaker for handling of oversize fragments. Atlas Copco make D50 and Sandvik make TITON 500 drill machine is being used regular drilling and blasting operation with 9 to 10 m bench height. Burden varied between 3 and 3.5 m, spacing between 4 and 5 m and quantity of charge per hole between 40kg & 60 kg for 115 mm drill diameter. Accordingly, the stemming column in the blast holes also varies between 2.5m to 3.0 m. Staggered pattern and square grid pattern of holes are drilled. The blast hole depth is 10 meter including 10% sub grade drilling. The non-electric (NONEL) system of initiation (TLDs 17/250ms and 25/250ms) is being used for blasting work in combination with ANFO and cast booster weighing 150 gm. In case of watery hole during the rainy season and in the lower bench Large diameter slurry explosive cartridge (Aquadyne and supergel) is used for blasting. Each blast is monitored for ground vibration and fragmentation and necessary care is taken based on the report obtained. Minimate is used for measurement of ground vibration in the mines.

In blasting, two to three rows of holes are blasted at a time and maximum of 60 holes are blasted at a time. With proper initiation pattern, charging pattern and charge per delay. Ground vibration is maintained within 3.00mm/s within 300 meter of the blasting site. A sample initiation pattern given below depicts the basting of each hole one after another. General blasting pattern followed in the mine, charging pattern and charging with supergel exlosive are shown in Figure 12, 13 and 14 respectively. Table 4 shows observations recorded at Dunguri Limestone Mine.

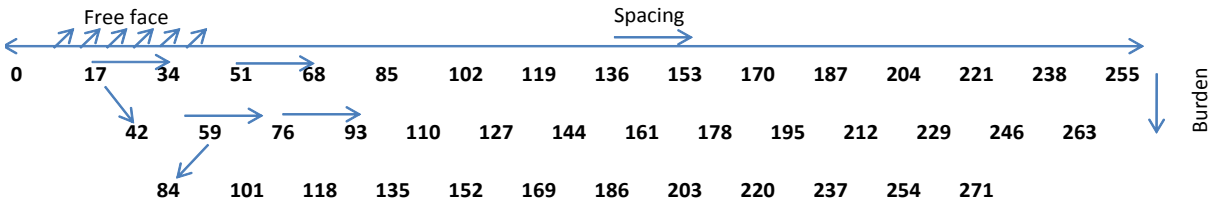

In a row hole to hole delay 17ms.
Row to row delay betweeen 2nd hole of the 1st row and 1st hole of the 2nd row is 25ms
Row to row delay betweeen 2nd hole of the 2nd row and 1st hole of the 3rd row is 25ms
Spacing 3.0 meter to 4.5 meter
Burden 2.5 meter to 3.0 meter

Fig 12: General blasting pattern followed at Dunguri mine (ACC)

Delay is set in such a way that each hole gets the adequate free face and blasted at a time. Hence optimum fragmentation with reduced ground vibration is achieved. So practically the charge per delay is only the amount of explosive placed in a single hole, i.e. 40 to 60kg. The village Dungri is situated at a distance of 850 meter from the active mine. (Quarry No 6). The mine is equipped with two explosive magazine of 5.6 ton each and an ammonium nitrate store house of 45 Ton capacity. The detonator storage capacity of the magazines is 30,000 numbers for each magazine. One road van of 2.6ton capacity is present for transportation of explosive.

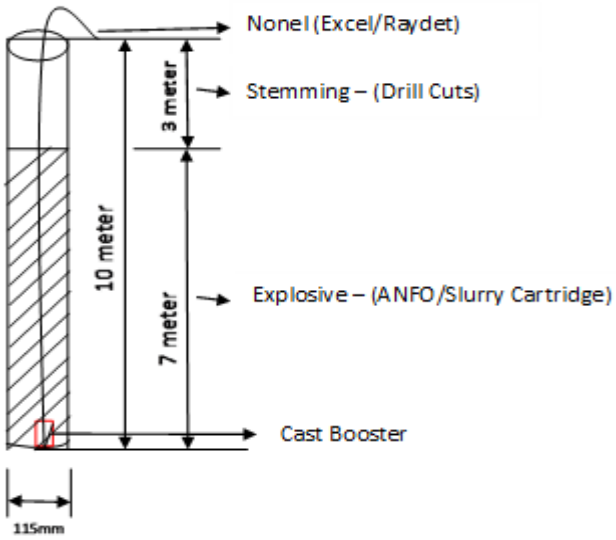

Fig 13: General charging pattern followed at Dunguri mine (ACC)

Fig 14: Charging of blast hole with Supergel explosive at Dunguri mine (ACC)

4.1.2 OBSERVATIONS RECORDED AT DUNGURI LIMESTONE MINE

Table 4: Observations recorded at Dunguri Limestone Mine

Sl No	Distance (m)	Hole Depth (m)	Charge per hole (kg)	Burden (m)	Spacing (m)	No of holes	Total Explosive charge (kg)	Peak Particle Velocity (mm/s)	Dominant Frequency (Hz)
1	500	10	50	3	4	64	3200	1.62	21.5
2	150	10	50	4	5	67	3350	4.16	19.8
3	300	10	50	4	3	99	4950	3.52	2
4	200	10	50	3	4	15	750	2.52	2.25
5	400	9	55	3	5	80	4400	2.05	11.3
6	500	9.5	55	4	3	40	2200	1.33	24
7	600	10	30	3	4	96	2880	0.873	25.3
8	750	9.5	36.46	2.5	4	55	2005	0.191	18.3
9	150	9.5	50	4	3	130	6500	8.60	2.25
10	500	10	50	4	3	58	2900	3.10	34.3
11	150	9	34.6	4	3	63	2180	6.10	17.8

4.2 IDL EXPLOSIVES LIMITED

4.2.1 Details of blasting for the purpose of metal cladding

The blast site is located in the coordinates 22°11'12.8"N 84°52'28.4"E falling in Sonaparbat area near IDL colony, Rourkela, Sundergarh district, Odisha. IDL Explosives Limited is one of the leading manufacturers of industrial explosives of India and caters the needs of various mines of the country. Explosion clad plates are also being manufactured which are used in various applications like chemical, petrochemical, ship building, smelters etc., Cladding is being conducted on sand base surface which is spread uniformly and the plates are cladded with the help of explosives in form of powder which is initiated by remote device. The pressure released from this cladding by the explosives joins two different metal plates. This process generates sound /air

blast effect in the surroundings. The cladding plate is placed over the backer plate with a small gap between the two. A layer of specially prepared explosive charge is spread on top of the cladding plate. On detonation the cladding plate collides progressively with the backer plate at a high velocity. This collision is completed in milli seconds and removes the contaminating surface films like oxides and adsorbed gases in the form of a line jet at collision front thereby bringing together two virgin metal surfaces to form a metallurgical bond by electron sharing. Figure 15 shows the preparation of blast with powder explosive for metal cladding at IDL –Explosives Limited-Rourkela.

Fig 15: Preparation of blast with powder explosive for metal cladding at IDL –Explosives Limited-Rourkela

4.2.2 OBSERVATIONS RECORDED AT IDL EXPLOSIVES LTD. ROURKELA

Table 5: Observations recorded at IDL explosives Ltd. Rourkela

Blast No	Explosive Charge (kgs)	Distance from the blast (m)	Peak Particle Velocity (mm/s)	Frequency
1	300	500	2.11	74
2	200	720	0.32	13.6
3	90	650	0.44	15.5
4	150	1500	0.238	11.8
5	100	800	0.25	18.8
6	270	2750	0.238	11.8
7	270	1990	0.683	22.6
8	50	564	0.349	14.3

9	530	1520	0.381	19.6
10	180	493	1.11	30.6
11	540	1320	0.286	29
12	195	777	0.714	29
13	540	750	0.33	19
14	540	354	1.71	42.8
15	240	390	2.27	10.3
16	270	2700	0.91	11.8
17	240	800	1.86	11.2
18	240	1000	1.51	9.8
19	240	1000	1.81	13.6
20	240	1200	1.02	17.1

4.3 BAPHLIMALI BAUXITE MINE (UAIL)

4.3.1 BLASTING PRACTICES AT THE MINE

Baphlimali Bauxite Mines under M/S Utkal Alumina International Limited have started mining operation since Nov'12. The hill is essentially composed of khandalites with charnockites occurring in the south-eastern part of the hill. The formations have NE-SW trends and steep south-easterly dips of 50-80 degrees. Baphlimali Bauxite deposit extends over an area of 9.68 sq. km and roughly corresponds to an ovoid of 6.3 km * 3.2 kms size. It is a blanket type of deposit having average 10 -12 m hard laterite as overburden and thickness of Bauxite varies from 10-12 m.

At present, conventional explosives are being used for blasting operations and it is proposed to introduce slurry mix emulsion explosive as column charge and Emul Boost as cast booster as an alternate and improved methodology. In this regard, Management of M/S UTKAL ALUMINA INTERNATIONAL LIMITED wanted to conduct scientific study for understanding the effect of blasting in the geomining conditions of the Baphlimali Bauxite Mines. Some of the geotechnical data available with the mines and with the explosive manufacturers M/s Keltech Energies Ltd was utilized for the analysis. Figure 17 & 18 shows the charging pattern and charging of blasthole with SME respectively.

The deposit covers an area of 9.68 sq. Km occurring as a residual blanket-type deposit over the khondalite basements, on top of the Baphlimali plateau. The plateau boundary roughly resembles the map of India and is oval in shape with maximum dimensions of 6.3 km and 3.2 km. It rises to about 150-200 m above the surrounding valleys. It is bounded by 19°18' to 19°22' North latitudes

and 82°57' to 82°59' East longitudes and forms a part of survey of India topo- sheet no. 65 1/15. The major axis of the plateau trends a bearing of N 40°30'E.

4.3.2 Mining Method

Mining method adopted for a deposit is largely influenced by the geology, geomorphology, overburden to ore ratio, rock properties spatial distribution of ore, production level, quantity of overburden, quality required, environmental considerations, climatic conditions of the area etc. Figure 16 shows the location of site of experimental blast at UAIL and table 6 shows the observations recorded at UAIL.

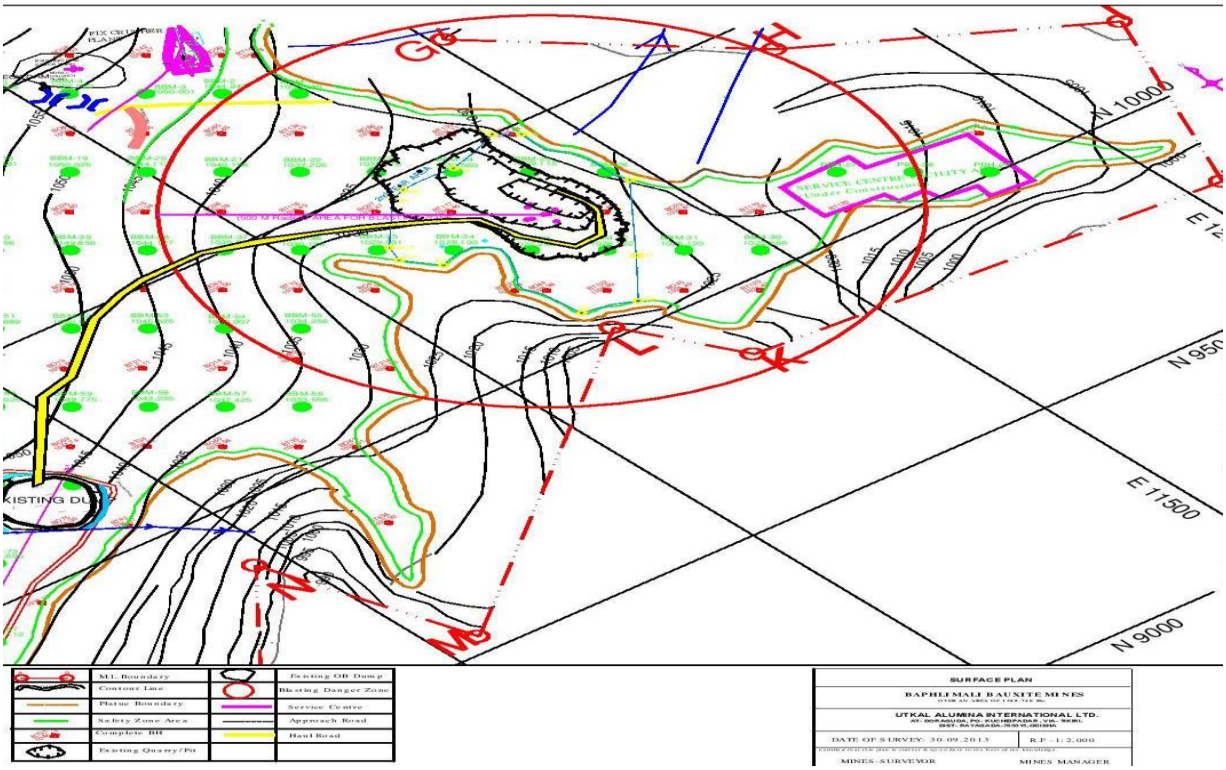

Fig 16: Mine Plan showing location of site of experimental blast at UAIL.

Trench mining method of mining known as trench method is adopted for this deposit. In this method, mining fronts are planned to advance roughly parallel to the contours. Mining at this deposit involves –

- Removal of the OB/waste covers lying on top of the bauxite layer.

- Excavation of bauxite
- Mining of bauxite close to the floor
- Back-filling of OB/waste into mined out areas for land reclamation.
- This being a plateau top deposit, a 15 m wide peripheral zone of un-mined bauxite is proposed to be left on the edge of the plateau. This will act as a peripheral barrier for the purpose of equipment safety, avoiding discharge of silts into the surrounding valleys directly, and hiding the mining activities from adjacent areas.

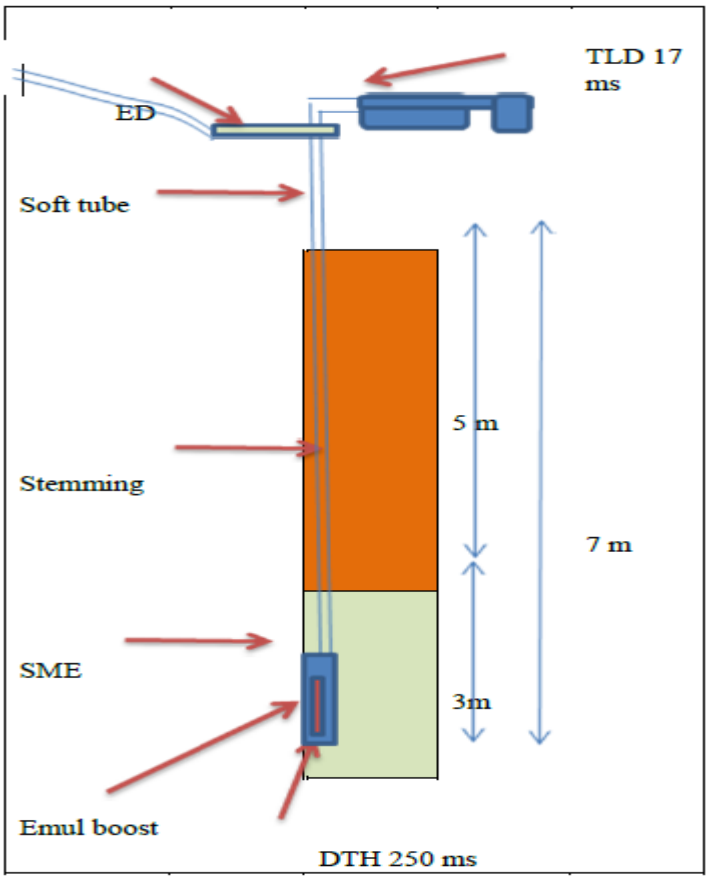

Fig 17: Charging pattern of blasthole with SME

Fig 18: Charging of SME in the blast hole

4.3.3 OBSERVATIONS RECORDED AT UAIL

Table 6: Observations recorded at UAIL

Sl No.	Distance	Charge per hole	Charge per Delay	Hole Depth	Burden (m)	Spacing (m)	No of holes	Total Qty of Explosive used (kg)	PPV (mm/s)	Frequency (Hz)
1	160	65	520	6.5	3.5	4	62	4030	6.51	12.5
2	160	30	480	5.5	2.5	3	108	3240	3.8	17.7
3	160	40	320	5.5	3.5	4	122	4880	3.94	4.8
4	130	55	440	6	3.5	4	109	5995	7.35	11.3
5	130	50	150	5.5	3.5	4	87	4350	6.01	12.8
6	130	40	120	5.5	3.5	4	39	1560	3.21	9.9

7	150	55	440	5.5	3.5	4	130	7150	12.2	8.8
8	150	55	440	6	3.5	4	52	2860	4.24	11
9	175	50	50	6	3.5	4	55	2750	5.32	7.5
10	150	55	110	6	3.5	3	110	6050	8.81	6.6
11	130	55	55	6	4	5	59	3245	8.61	7.1
12	150	80	320	8	4	5	57	4560	5.55	6.1
13	150	60	60	6	3.5	4.5	107	6420	13.4	9.5
14	100	70	70	7	3.5	4	75	5250	13.1	12
15	175	68	68	7	3.5	4.2	73	4964	3.51	7.9
16	100	70	140	7	3.5	4.2	38	2660	12.2	8.6
17	175	70	70	7	3.5	4.2	115	8050	6.18	11.9
18	150	30	30	6	2.5	4.2	19	570	4.49	8.6
19	100	70	210	7	3.5	4.5	63	4410	4.87	7.6
20	150	65	130	7	3.5	4.5	86	5590	10.21	13.3

CHAPTER-5
RESULTS AND COMPARISON

RESULTS AND COMPARISON

5.1 DUNGURI LIMESTONE MINE, ACC

The number of input parameters taken were six for ANN and MVRA. They were distance, hole depth, charge per hole, burden, spacing and no of holes. An error tabulation was generated between the recorded and predicted PPV. Table 7 shows the error calculation of PPV predicted by both ANN & MVRA. It shows that the error generated from prediction in ANN is lesser than the statistical analysis. The maximum and minimum error generated by ANN was 0.5992 and 0.1688 respectively whereas the maximum and minimum error generated by MVRA was 2.4712 and 0.6502 respectively. Figure 19 & 20 show the regression analysis of ANN and MVRA. The correlation coefficient determined by ANN & MVRA was 0.9322 and 0.6833 respectively. Figure 21,22 and 23 show the line graph comparison between the recorded and predicted PPV by ANN and MVRA. Figure 24 shows the bar graph comparison between the recorded and predicted PPV by ANN and MVRA.

Table 7: Error calculation of PPV predicted of ACC by ANN & MVRA

Sl no.	Recorded PPV	Predicted PPV by ANN	Standard Deviation	Predicted PPV by MVRA	Standard Deviation
1	1.62	1.4166	0.2034	0.9698	0.6502
2	4.16	3.9887	0.1713	2.9968	1.1632
3	3.52	3.8264	0.3064	5.0004	1.4804
4	2.52	2.2262	0.2938	3.9994	1.4794
5	2.05	2.4248	0.3748	0.9898	1.0602
6	1.33	1.4988	0.1688	2.9854	1.6554
7	0.873	0.4962	0.3768	1.9684	1.0954
8	0.191	0.4122	0.2212	2.0012	1.8102
9	8.60	8.0008	0.5992	6.1288	2.4712
10	3.10	3.6254	0.5254	4.9866	1.8866
11	6.10	6.6888	0.5888	4.1212	1.9788

The equation for prediction of PPV by MVRA is:

PPV = 15.33644 -0.00874 (Distance) -0.75903(Hole depth) -0.00965 (Charge per Hole) + 0.035712 (Burden) – 0.84386 (Spacing) +0.027468 (No of holes)
…… (5.1.1)

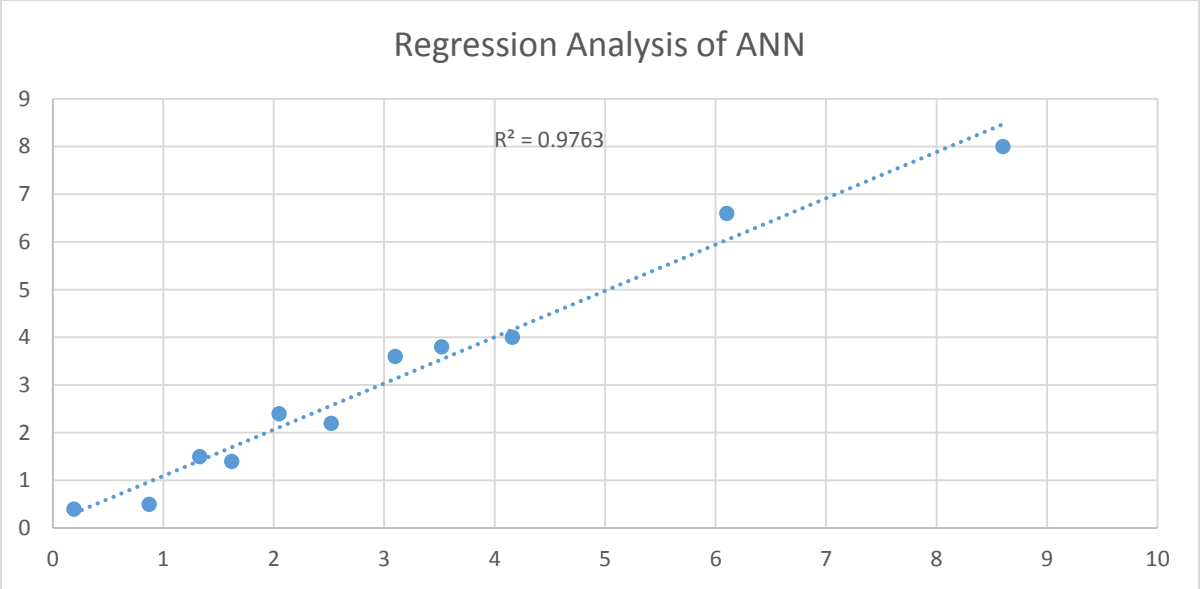

Fig 19: Regression analysis between recorded and predicted PPV of ACC by ANN

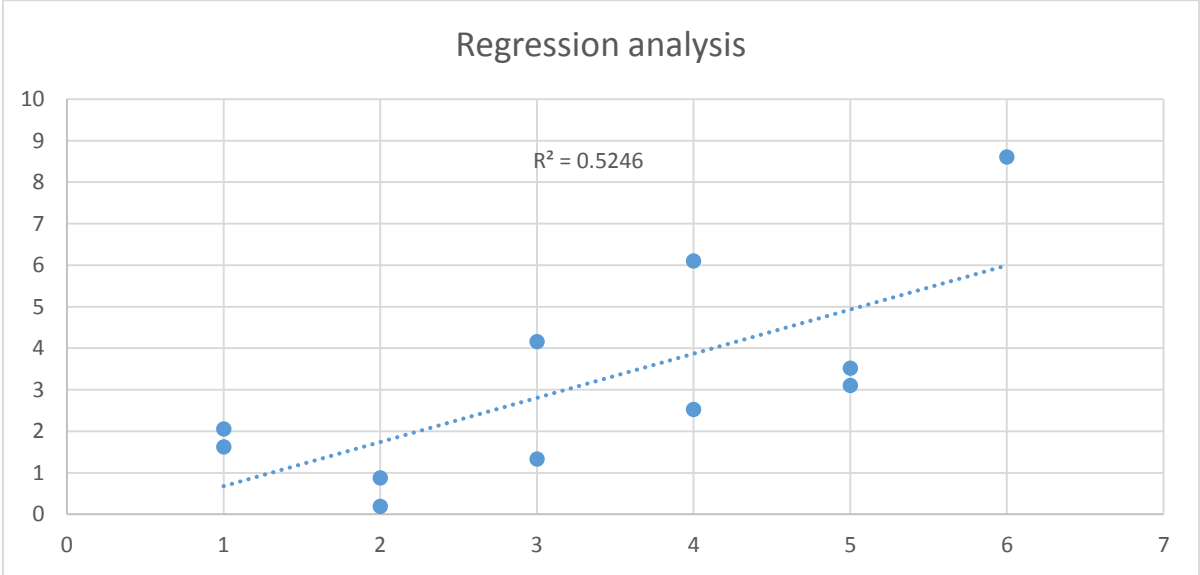

Fig 20: Regression analysis between recorded and predicted PPV of ACC by MVRA

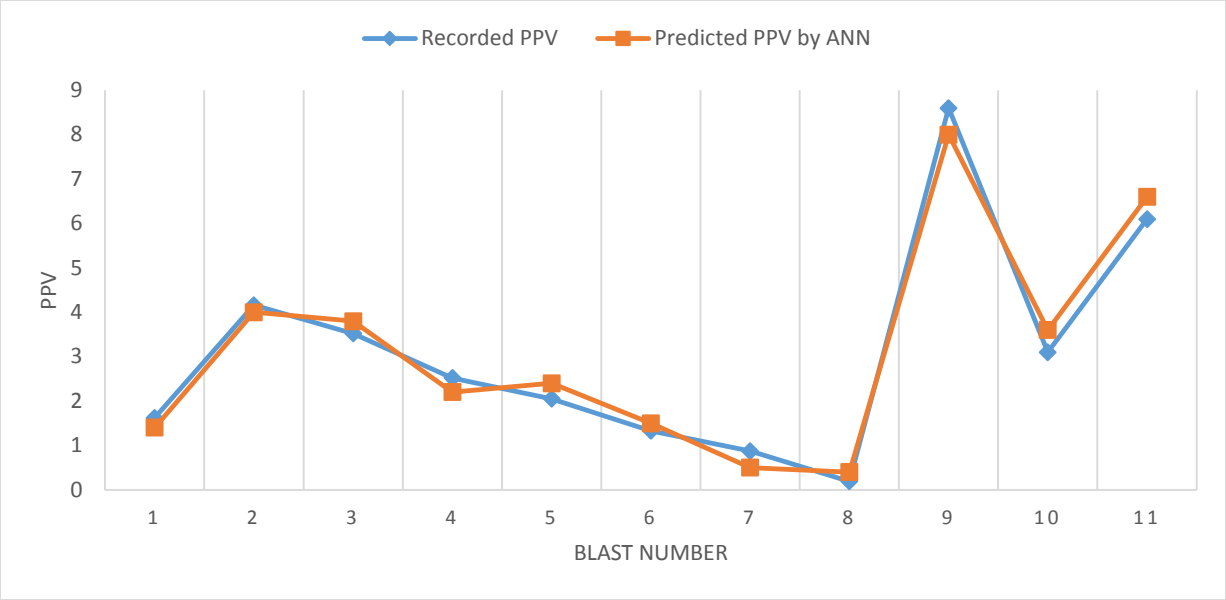

Fig 21: Line graph comparison between recorded and predicted PPV of ACC by ANN

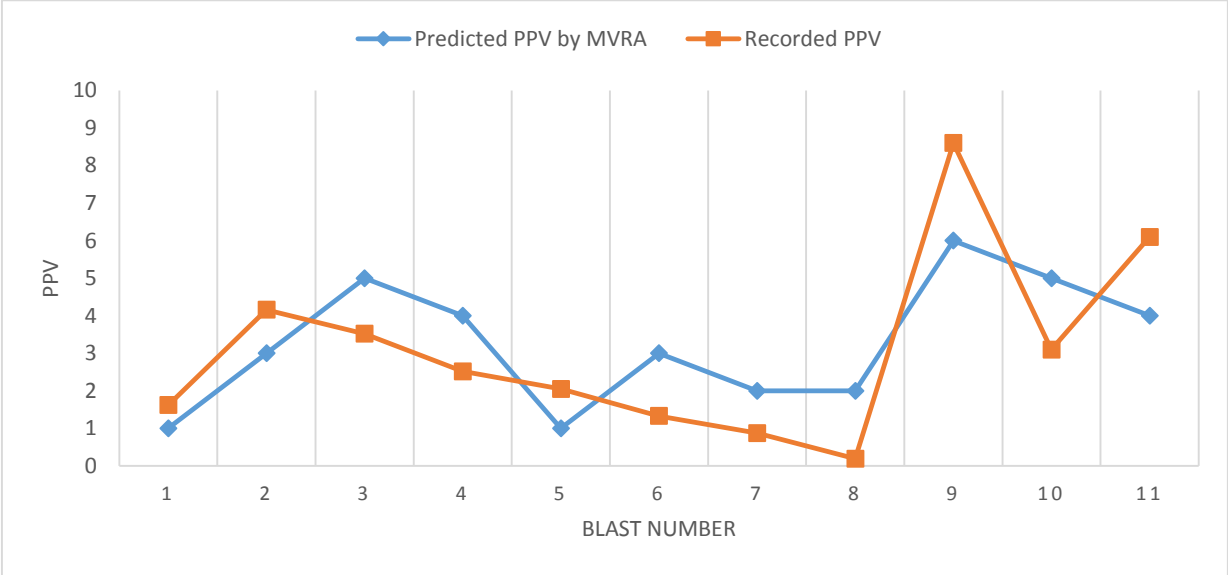

Fig 22: Line graph comparison between recorded and predicted PPV of ACC by MVRA

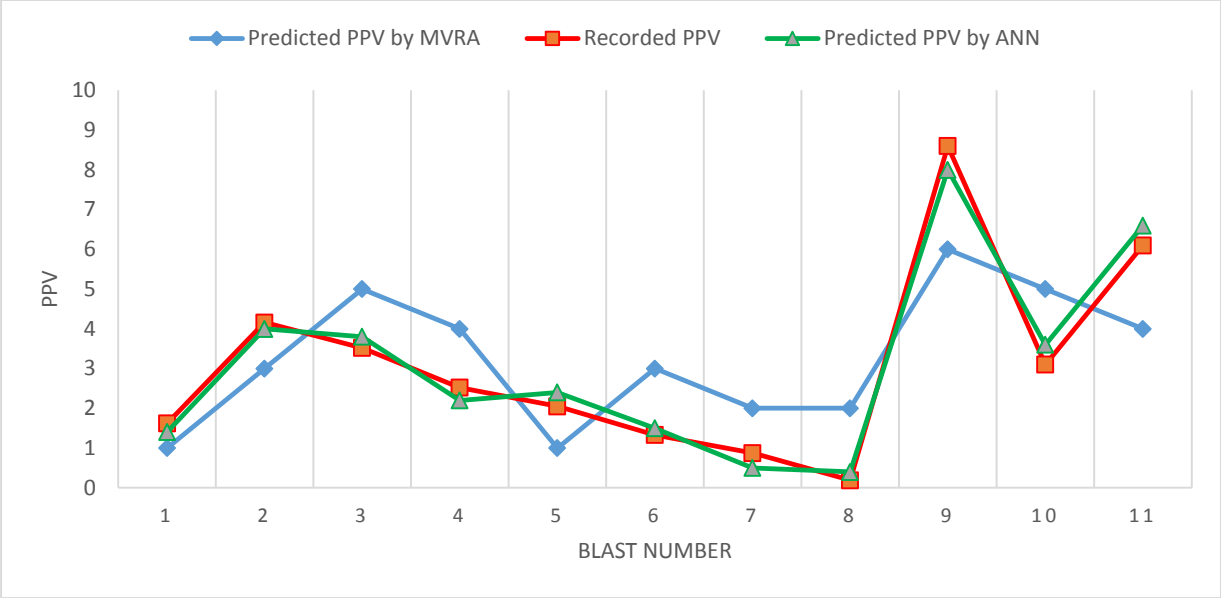

Fig 23: Line graph comparison between recorded and predicted PPV of ACC by ANN & MVRA

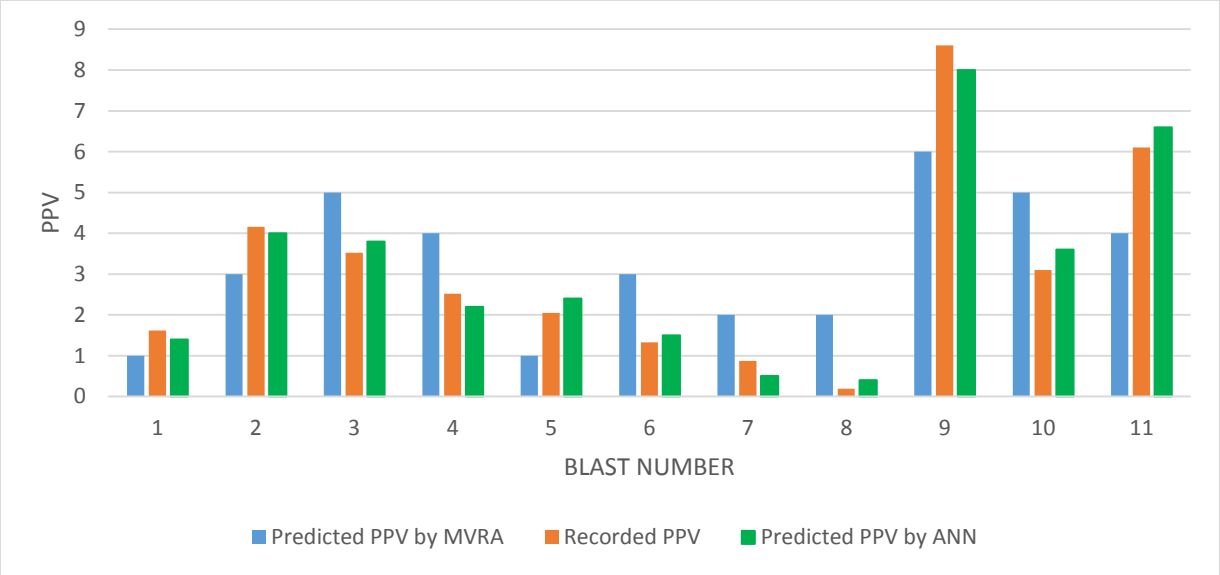

Fig 24: Bar graph comparison between recorded and predicted PPV of ACC by ANN & MVRA

The number of input parameters taken were six for ANN and MVRA. They were distance, hole depth, charge per hole, burden, spacing and no of holes. An error tabulation was generated between

the recorded and predicted frequency. Table 8 shows the error calculation of frequency predicted by both ANN & MVRA. It shows that the error generated from prediction in ANN is lesser than the statistical analysis. The maximum and minimum error generated by ANN was 2.9189 and 1.1382 respectively whereas the maximum and minimum error generated by MVRA was 6.6744 and 3.0213 respectively. Figure 25 & 26 show the regression analysis of ANN and MVRA. The correlation coefficient determined by ANN & MVRA was 0.9301 and 0.6667 respectively. Figure 27,28 and 29 show the line graph comparison between the recorded and predicted frequency by ANN and MVRA. Figure 30 shows the bar graph comparison between the recorded and predicted frequency by ANN and MVRA.

Table 8: Error calculation of Frequency predicted of ACC by ANN & MVRA

Sl no.	Recorded Frequency	Predicted Frequency by ANN	Standard Deviation	Predicted Frequency by MVRA	Standard Deviation
1	21.5	24.3662	2.8662	15.4554	6.0446
2	19.8	22.6872	2.8872	14.9999	4.8001
3	2	3.9668	1.9668	5.0213	3.0213
4	2.25	4.0236	1.7736	6.9299	4.6799
5	11.3	9.111	2.189	6.9396	4.3604
6	24	26.0874	2.0874	17.3256	6.6744
7	25.3	27.3232	2.0232	18.7562	6.5438
8	18.3	20.0064	1.7064	22.6484	4.3484
9	2.25	1.1118	1.1382	5.9284	3.6784
10	34.3	37.2189	2.9189	30.2141	4.0859
11	17.8	15.1864	2.6136	22.8632	5.0632

The equation for prediction of Frequency by MVRA is:

Frequency = -70.9841 +0.052424(Distance) +0.203808(Hole Depth) -0.46242 (Charge per Hole) +19.90629 (Burden) +6.850645 (Spacing) -0.12203 (No of holes) …… (5.1.2)

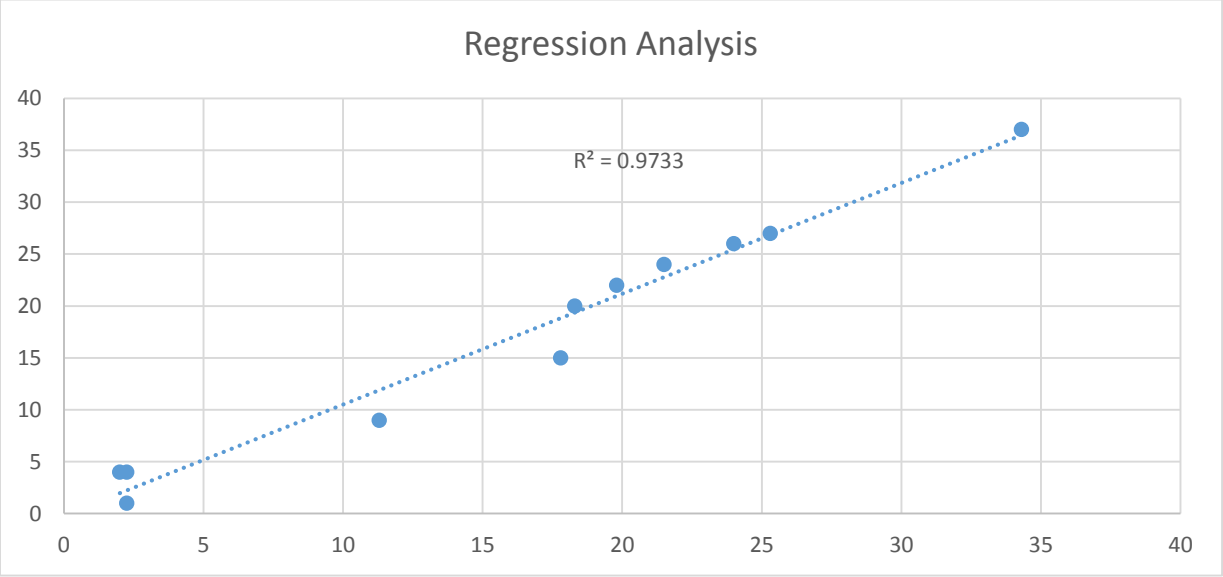

Fig 25: Regression analysis between recorded and predicted Frequency of ACC by ANN

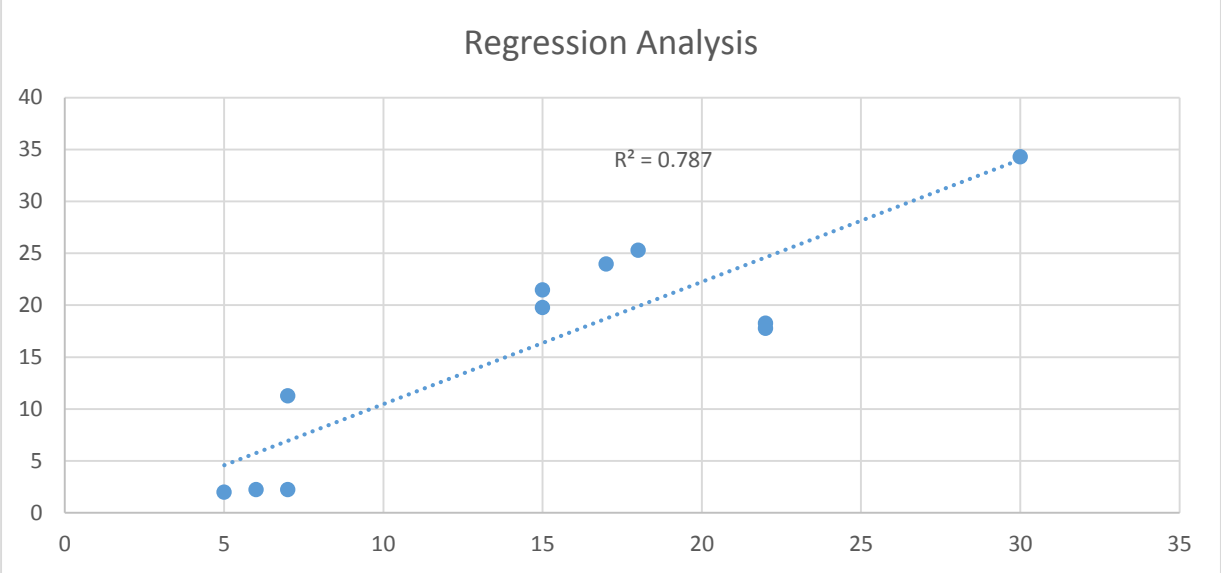

Fig 26: Regression analysis between recorded and predicted Frequency of ACC by MVRA

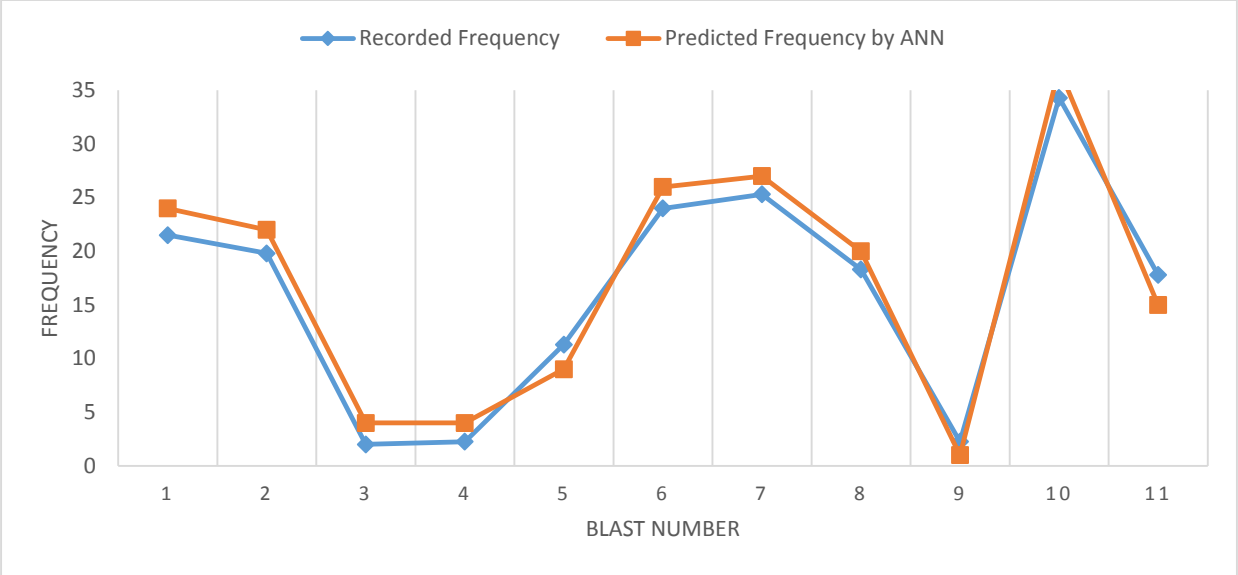

Fig 27: Line graph comparison between recorded and predicted Frequency of ACC by ANN

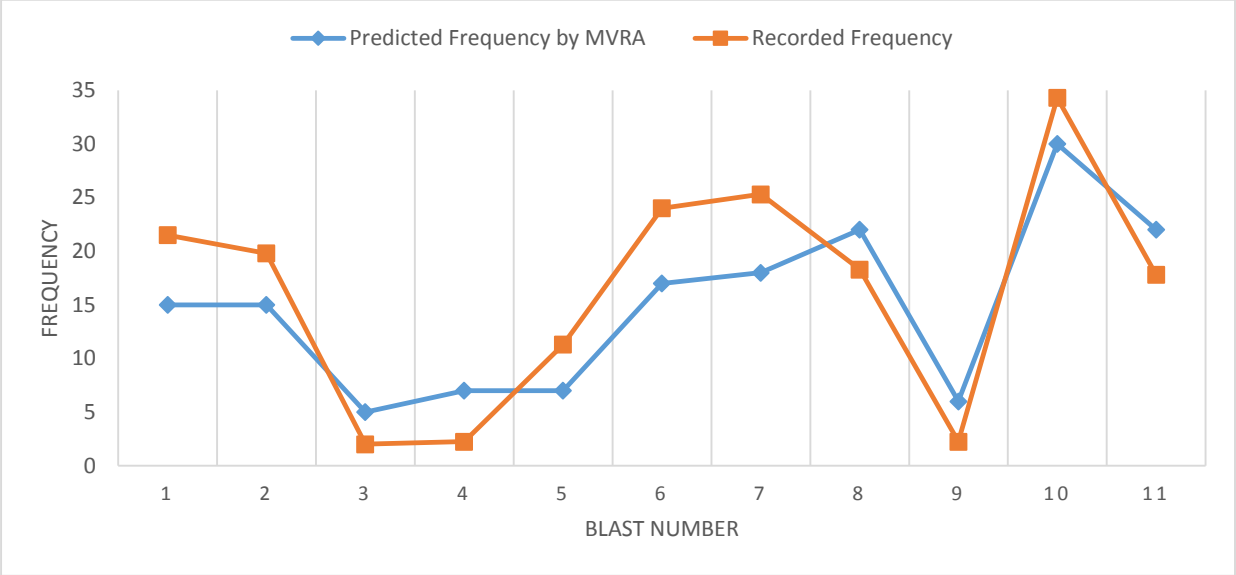

Fig 28: Line graph comparison between recorded and predicted Frequency of ACC by MVRA

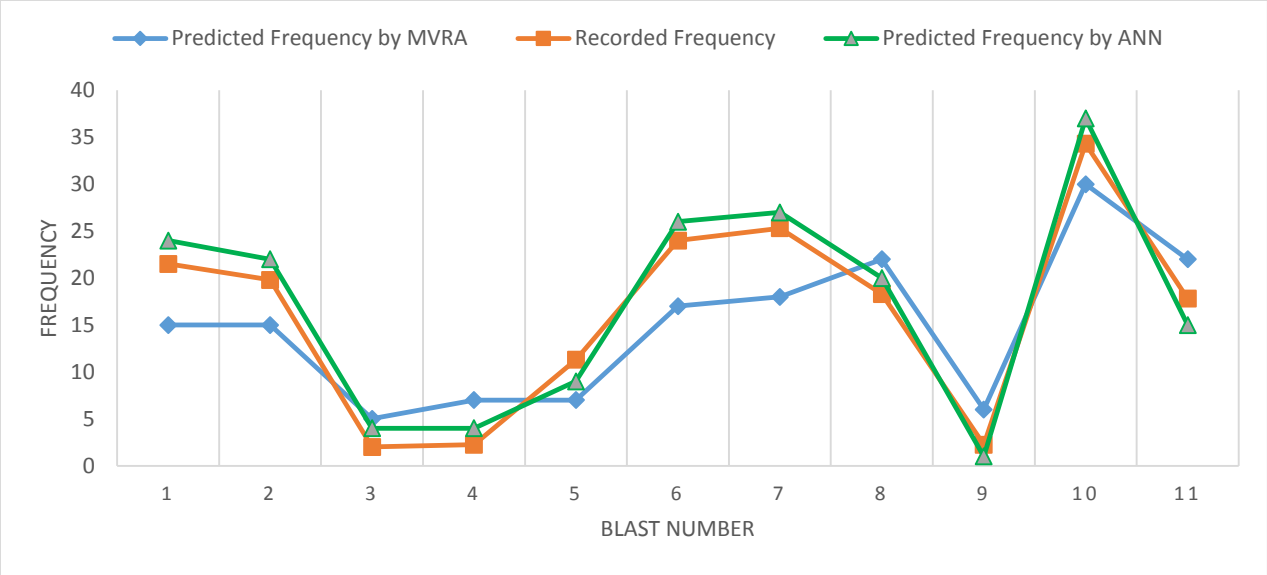

Fig 29: Line graph comparison between recorded and predicted Frequency of ACC by ANN & MVRA

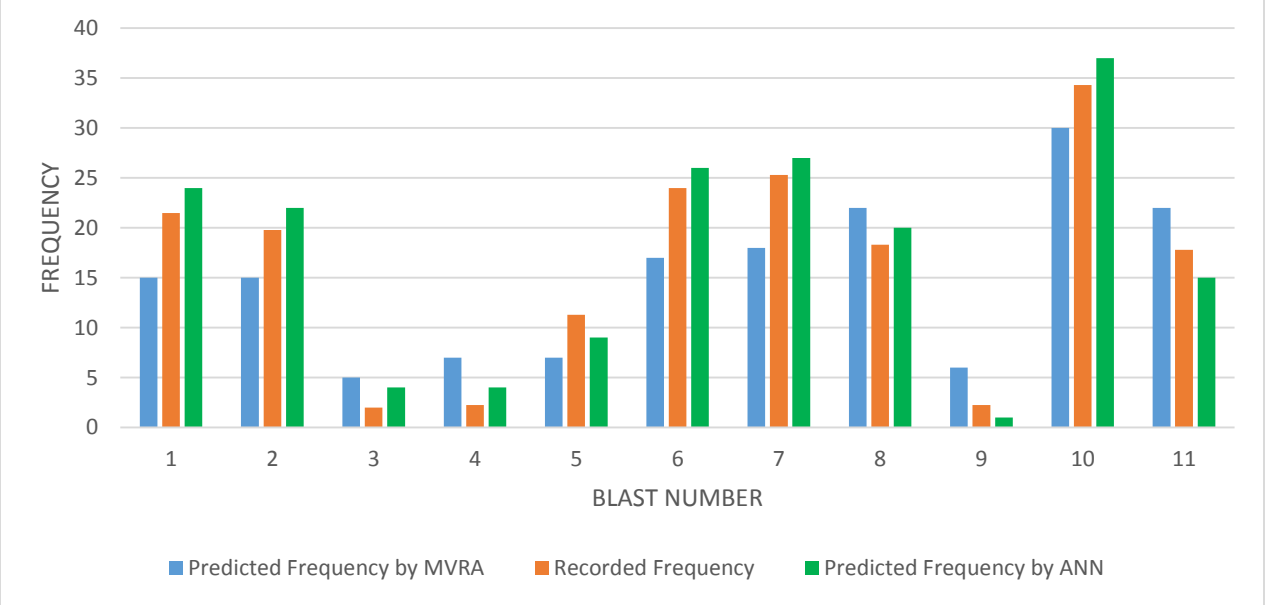

Fig 30: Bar graph comparison between recorded and predicted Frequency of ACC by ANN & MVRA

5.2 IDL

The number of input parameters taken were two for ANN & MVRA. They were distance and charge. An error tabulation was generated between the recorded and predicted PPV. Table 9 shows the error calculation of PPV predicted by both ANN & MVRA. It shows that the error generated from prediction in ANN is lesser than the statistical analysis. The maximum and minimum error generated by ANN was 0.4889 and 0.110 respectively whereas the maximum and minimum error generated by MVRA was 2.2641 and 0.4107 respectively. Figure 31 & 32 show the regression analysis of ANN and MVRA. The correlation coefficient determined by ANN & MVRA was 0.9053 and 0.5736 respectively. Figure 33, 34 and 35 show the line graph comparison between the recorded and predicted PPV by ANN and MVRA. Figure 36 shows the bar graph comparison between the recorded and predicted PPV by ANN and MVRA.

Table 9: Error calculation of PPV predicted of IDL by ANN & MVRA

Sl no.	Recorded PPV	Predicted PPV by ANN	Standard Deviation	Predicted PPV by MVRA	Standard Deviation
1	2.11	1.8988	0.2112	1.1122	0.9978
2	0.32	0.4996	0.1796	1.8832	1.5632
3	0.44	0.2984	0.1416	1.9088	1.4688
4	0.238	0.4986	0.2606	0.6487	0.4107
5	0.25	0.4998	0.2498	1.0538	0.8038
6	0.238	0.5023	0.264	0.9962	0.7582
7	0.683	0.5312	0.1518	1.993	1.3104
8	0.349	0.5148	0.1658	1.022	0.6736
9	0.381	0.5126	0.1316	1.0258	0.6448
10	1.11	0.9996	0.110	2.1533	1.0433
11	0.286	0.4953	0.2093	1.0287	0.7427
12	0.714	0.4962	0.2178	1.9985	1.2845
13	0.33	0.4982	0.1682	1.01	0.681
14	1.71	1.4874	0.2226	3.9741	2.2641
15	2.27	2.4899	0.2199	3.873	1.6032
16	0.91	0.6128	0.2972	1.9926	1.0826
17	1.86	1.9996	0.1396	3.0564	1.1964
18	1.51	1.9989	0.4889	3.0875	1.5775
19	1.81	2.0632	0.2532	2.9889	1.1789
20	1.02	0.8989	0.1211	2.9669	1.9469

The equation for prediction of PPV by MVRA is:

PPV = 1.236495 – 0.00039 (Distance) + 0.00043 (Explosive Charge) …… (5.2.1)

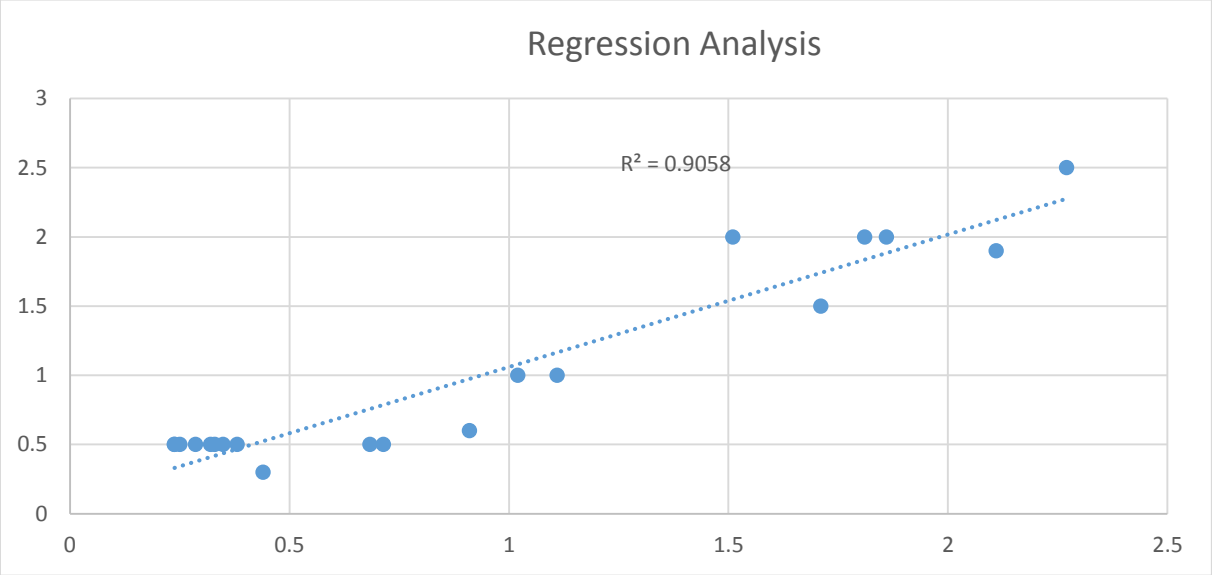

Fig 31: Regression analysis between recorded and predicted PPV of IDL by ANN

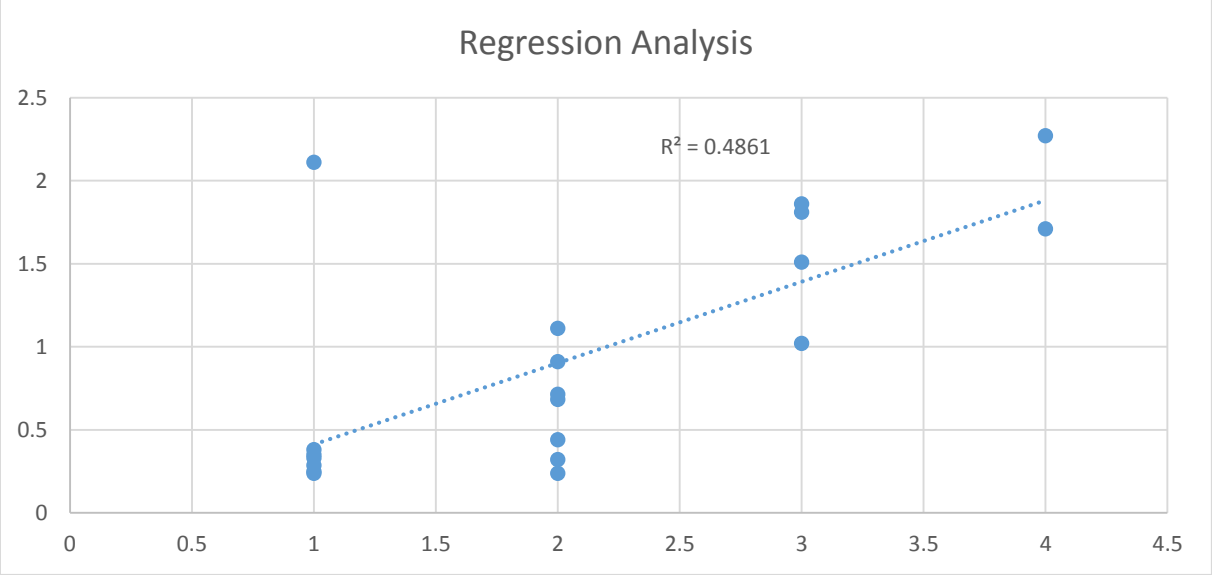

Fig 32: Regression analysis between recorded and predicted PPV of IDL by MVRA

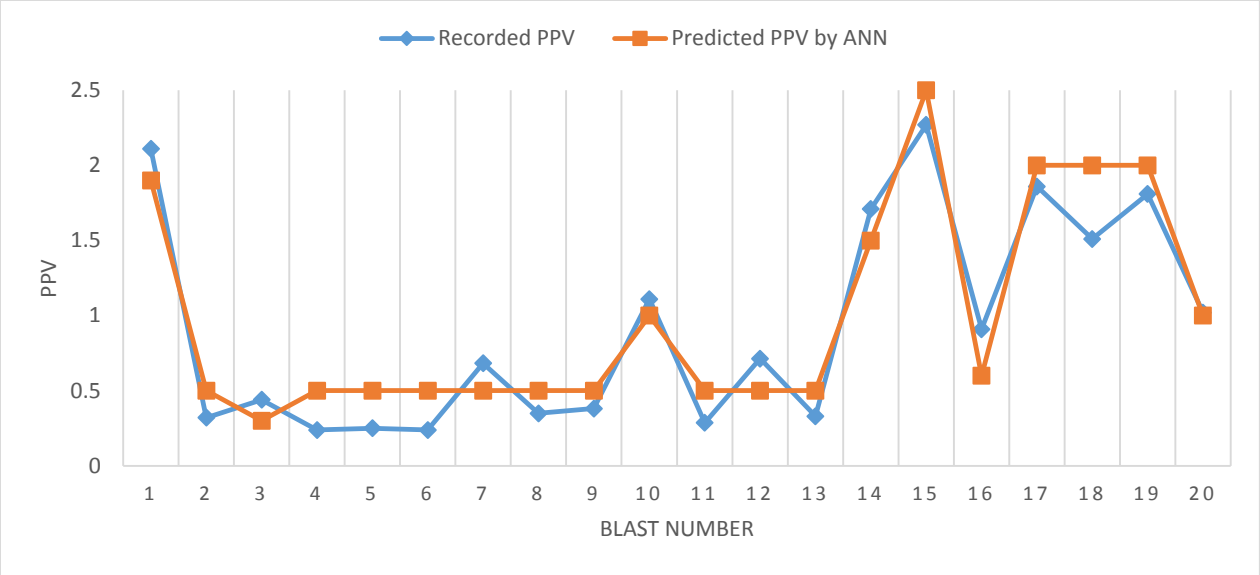

Fig 33: Line graph comparison between recorded and predicted PPV of IDL by ANN

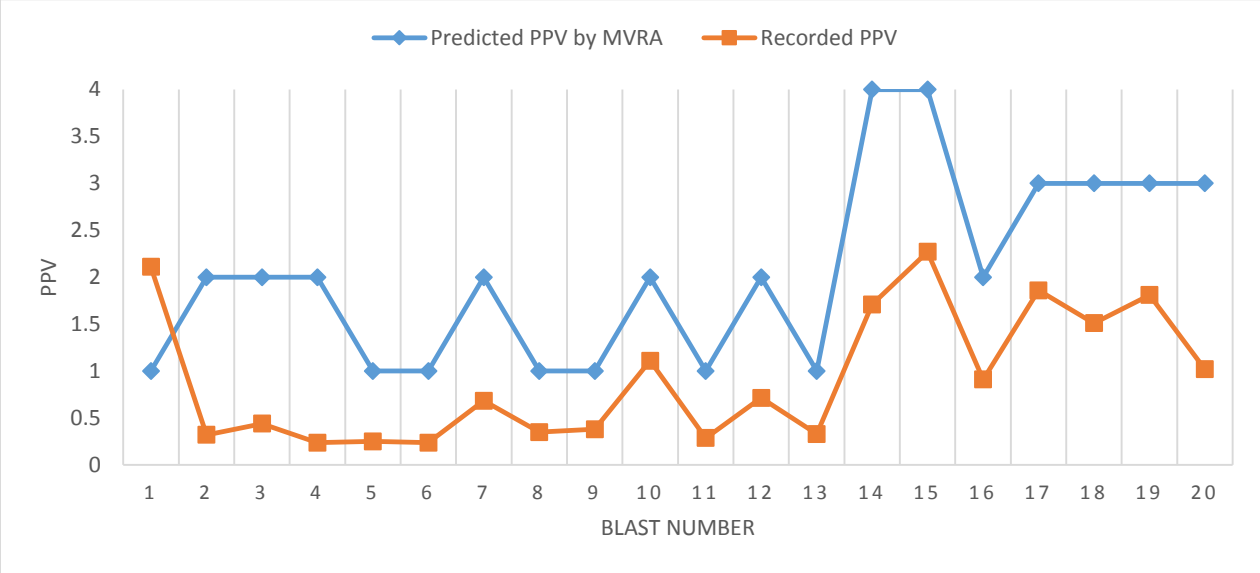

Fig 34: Line graph comparison between recorded and predicted PPV of IDL by MVRA

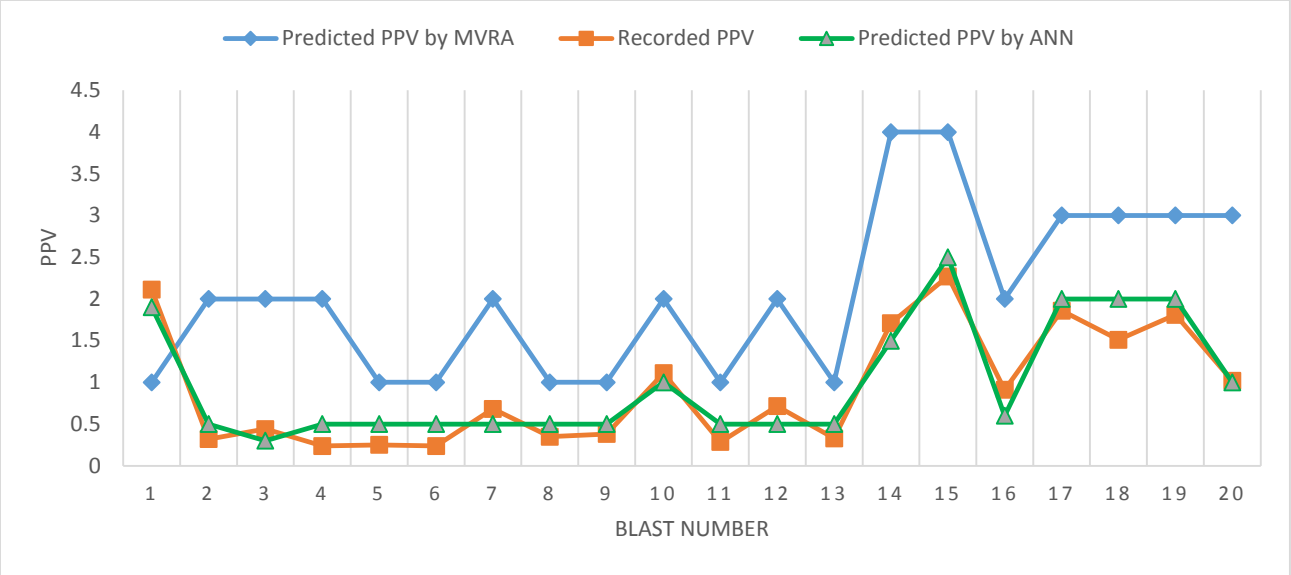

Fig 35: Line graph comparison between recorded and predicted PPV of IDL by ANN & MVRA

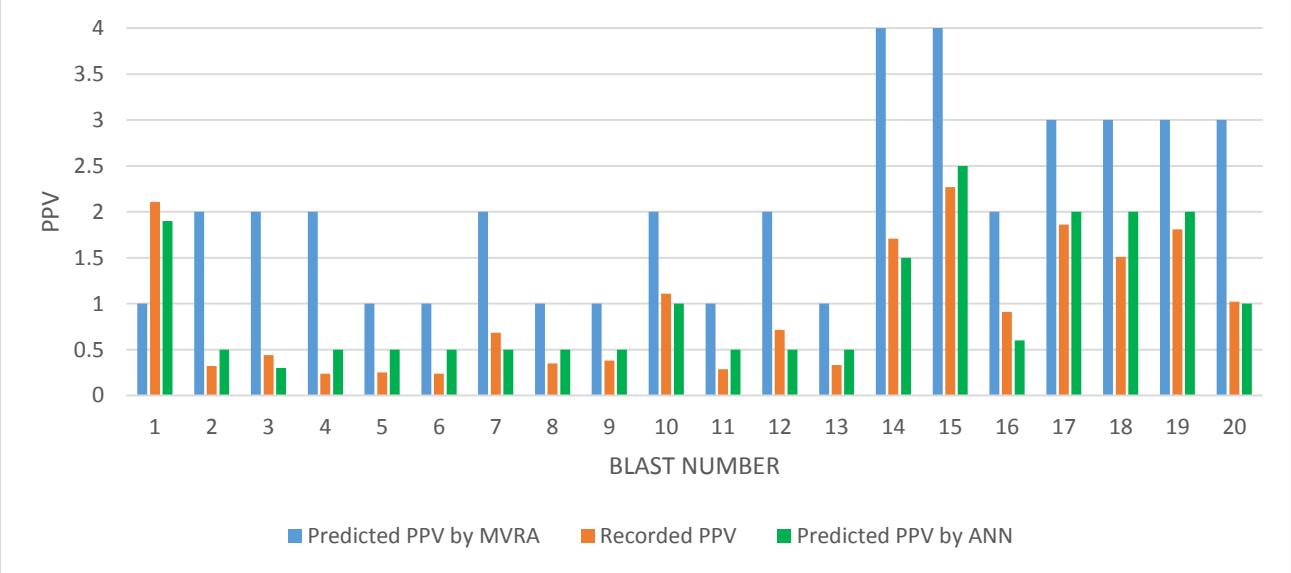

Fig 36: Bar graph comparison between recorded and predicted PPV of IDL by ANN & MVRA

The number of input parameters taken were two for ANN and MVRA. They were distance and charge. An error tabulation was generated between the recorded and predicted frequency. Table 10 shows the error calculation of frequency predicted by both ANN & MVRA. It shows that the error generated from prediction in ANN is lesser than the statistical analysis. The maximum and

minimum error generated by ANN was 3.6352 and 0.576 respectively whereas the maximum and minimum error generated by MVRA was 14.6744 and 2.0754 respectively. Figure 37 & 38 show the regression analysis of ANN and MVRA. The correlation coefficient determined by ANN & MVRA was 0.9136 and 0.6231 respectively. Figure 39, 40 and 41 show the line graph comparison between the recorded and predicted frequency by ANN and MVRA. Figure 42 shows the bar graph comparison between the recorded and predicted frequency by ANN and MVRA.

Table 10: Error calculation of Frequency predicted of IDL by ANN & MVRA

Sl no.	Recorded Frequency	Predicted Frequency by ANN	Standard Deviation	Predicted Frequency by MVRA	Standard Deviation
1	74	70.9991	3.0009	59.3256	14.6744
2	13.6	15.0564	1.4564	4.9898	8.6102
3	15.5	13.9996	1.5004	5.9675	9.5325
4	11.8	13.0587	1.2587	5.9937	5.8063
5	18.8	17.0699	1.7301	10.142	8.6573
6	11.8	13.2287	1.4287	15.6583	3.8583
7	22.6	20.0874	2.512	14.7806	7.8194
8	14.3	16.3754	0.576	14.8765	2.0754
9	19.6	17.0637	2.5363	14.5268	5.0732
10	30.6	32.4662	1.8662	24.9992	5.6008
11	29	27.1222	1.877	22.2823	6.7177
12	29	27.0928	1.9072	22.1264	6.8736
13	19	16.4823	2.5177	14.985	4.0147
14	42.8	39.164	3.6352	50.6628	7.8628
15	10.3	12.3394	2.0394	6.9986	3.3014
16	11.8	13.0642	1.2642	14.2234	2.4234
17	11.2	13.1264	1.9264	14.5399	3.3399
18	9.8	11.9997	2.1997	6.2255	3.5745
19	13.6	16.5239	2.9239	8.6729	4.9271
20	17.1	19.2121	2.1121	12.0761	5.0239

The equation for prediction of Frequency by MVRA is:

Frequency = 20.62364 - 0.00769 (Distance) + 0.033415 (Explosive Charge) …… (5.2.2)

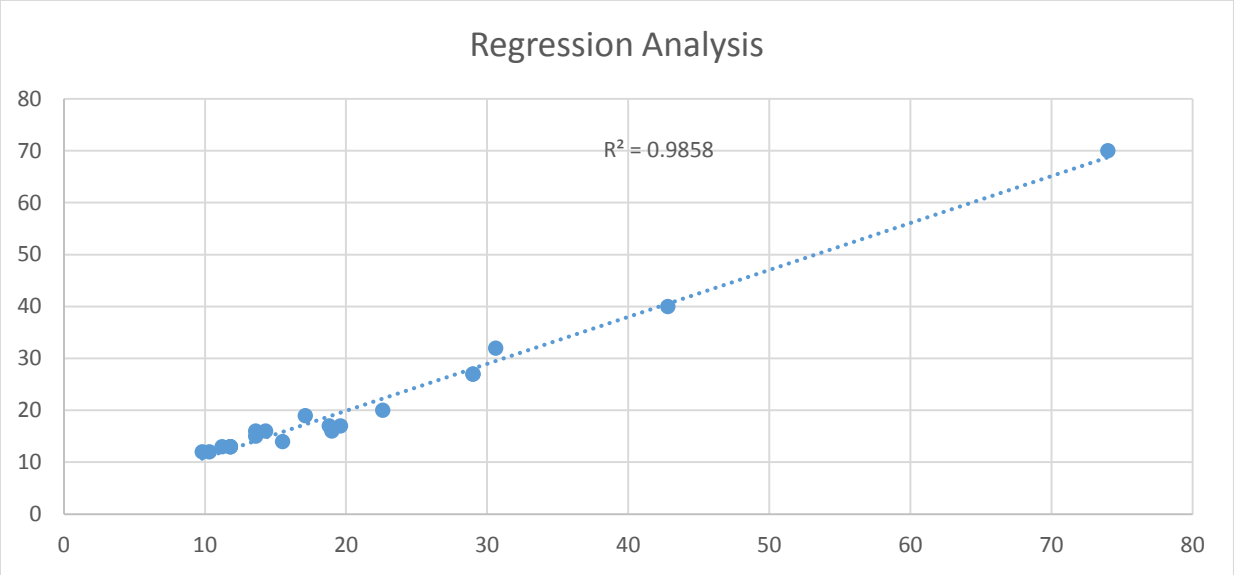

Fig 37: Regression analysis between recorded and predicted Frequency of IDL by ANN

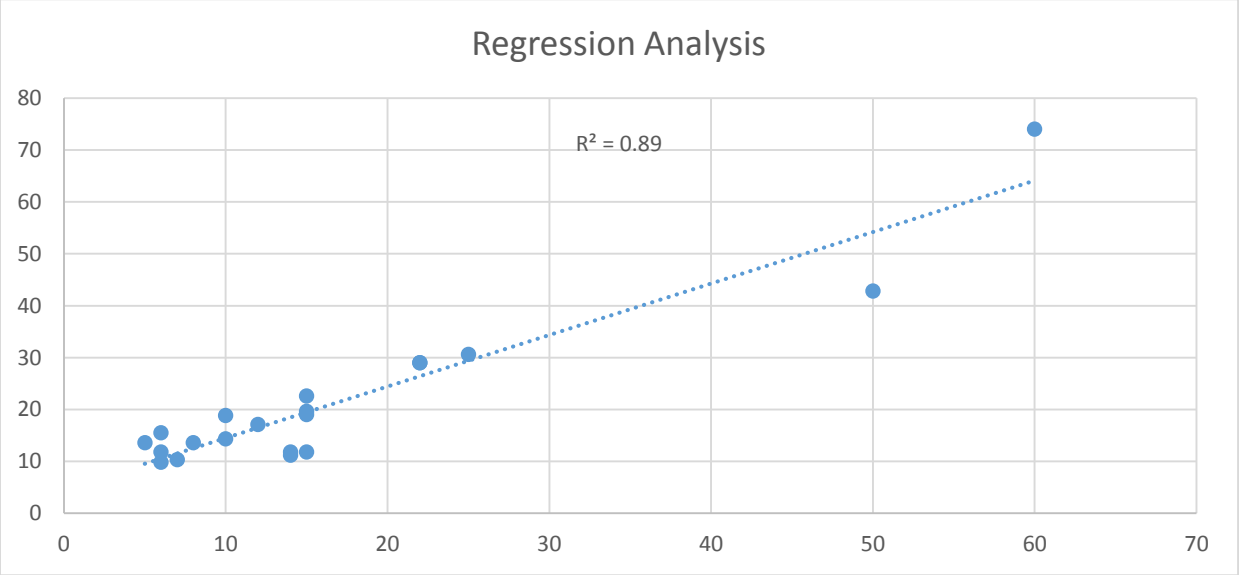

Fig 38: Regression analysis between recorded and predicted Frequency of IDL by MVRA

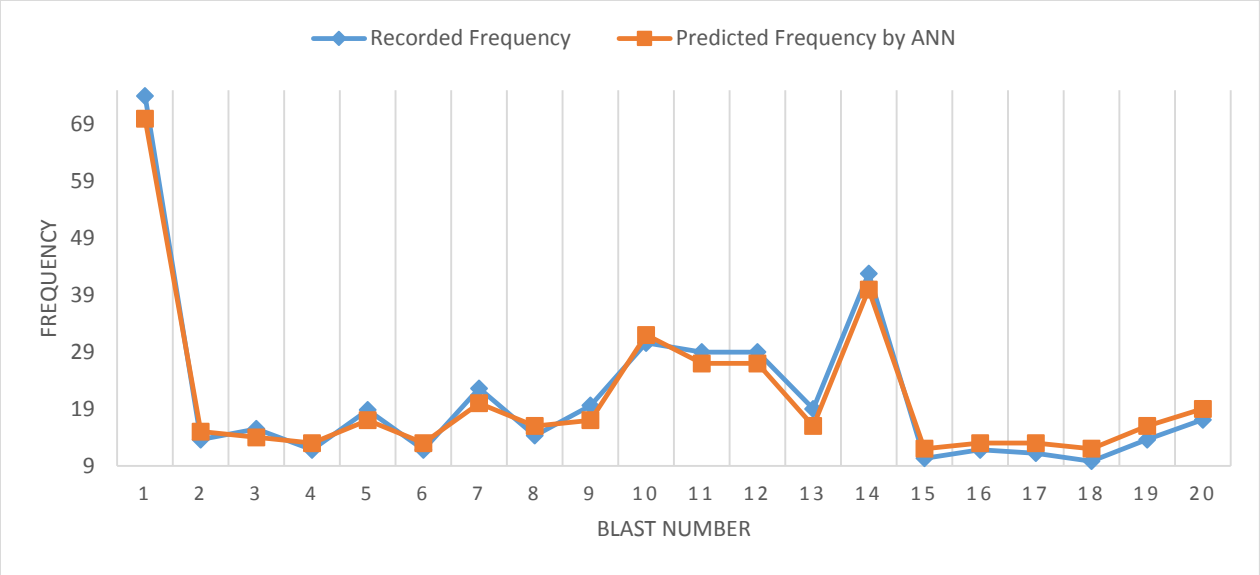

Fig 39: Line graph comparison between recorded and predicted Frequency of IDL by ANN

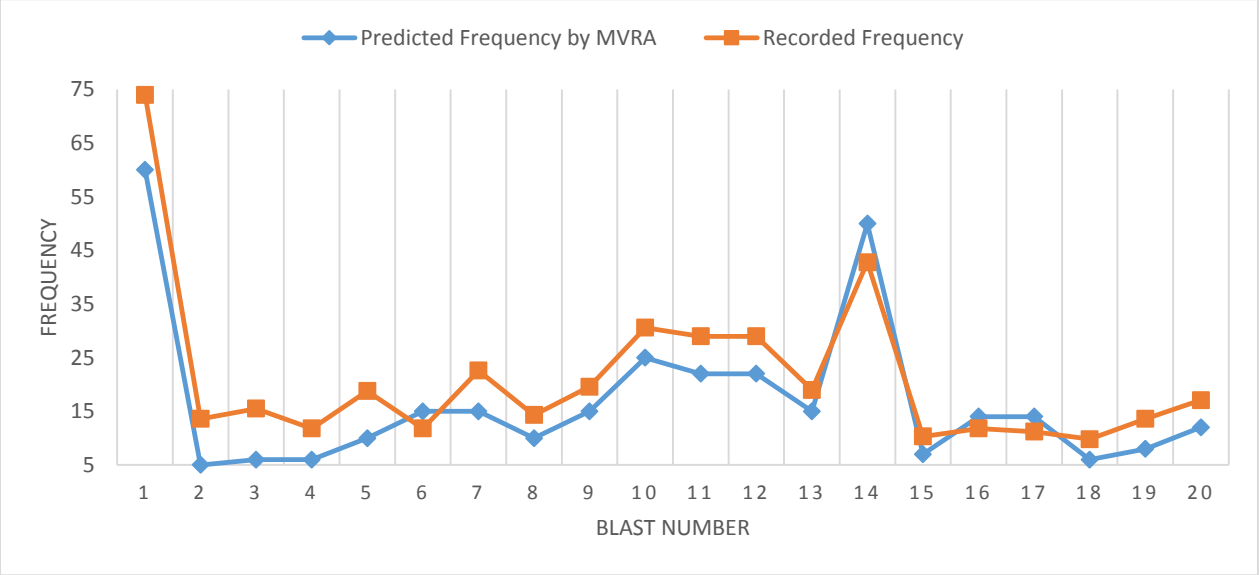

Fig 40: Line graph comparison between recorded and predicted Frequency of IDL by MVRA

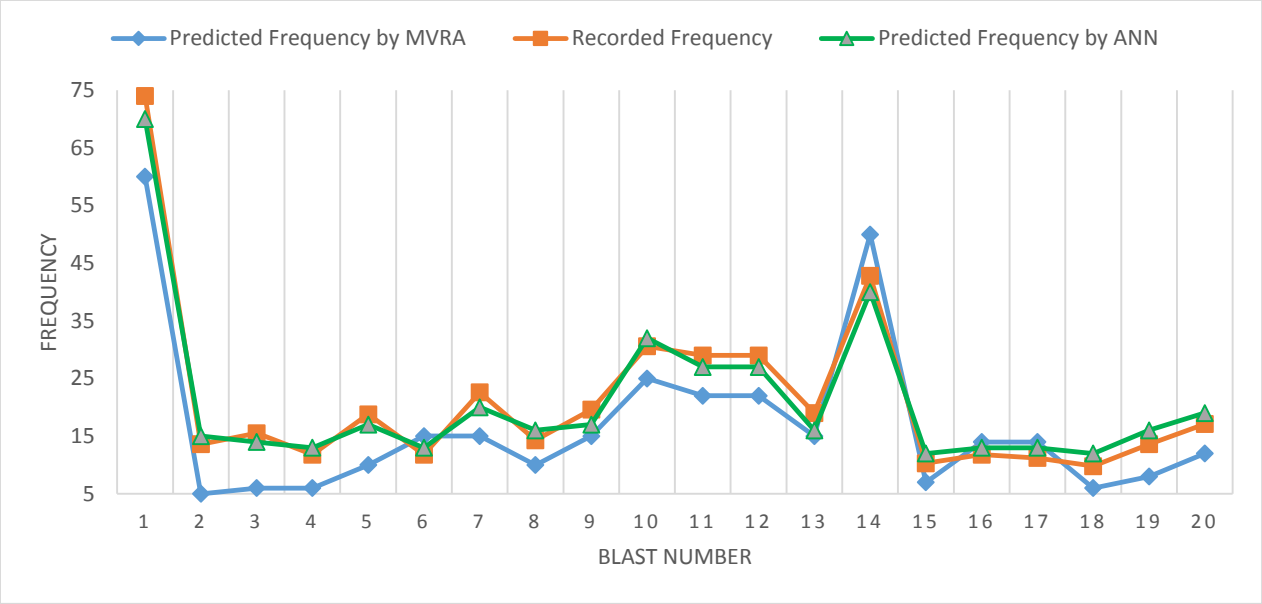

Fig 41: Line graph comparison between recorded and predicted Frequency of IDL by ANN & MVRA

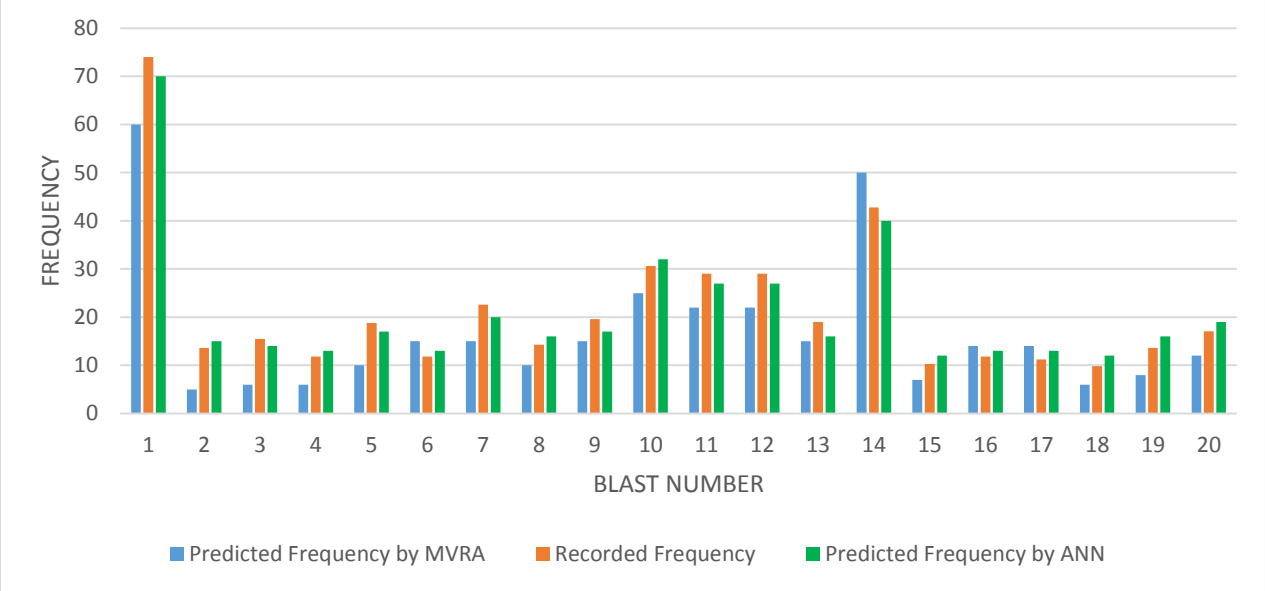

Fig 42: Bar graph comparison between recorded and predicted Frequency of IDL by ANN & MVRA

5.3 UAIL

The number of input parameters taken were six for both ANN and MVRA. They were distance, hole depth, charge per hole, burden, spacing and no of holes. An error tabulation was generated between the recorded and predicted PPV. Table 11 shows the error calculation of PPV predicted by both ANN & MVRA. It shows that the error generated from prediction in ANN is lesser than the statistical analysis. The maximum and minimum error generated by ANN was 1.2736 and 0.0018 respectively whereas the maximum and minimum error generated by MVRA was 4.0775 and 1.1533 respectively. Figure 43 & 44 show the regression analysis of ANN and MVRA. The correlation coefficient determined by ANN & MVRA was 0.9563 and 0.7477 respectively. Figure 45, 46 and 47 show the line graph comparison between the recorded and predicted PPV by ANN and MVRA. Figure 48 shows the bar graph comparison between the recorded and predicted PPV by ANN and MVRA.

Table 11: Error calculation of PPV predicted of UAIL by ANN & MVRA

Sl no.	Recorded PPV	Predicted PPV by ANN	Standard Deviation	Predicted PPV by MVRA	Standard Deviation
1	6.51	6.0991	0.4109	8.2999	1.7899
2	3.8	3.7982	0.0018	5.1634	1.3634
3	3.94	3.5463	0.3937	6.0202	2.0802
4	7.35	7.7426	0.3926	5.1769	2.1731
5	6.01	5.5842	0.4258	4.1208	1.8892
6	3.21	3.7329	0.5229	5.0284	1.8184
7	12.2	11.2586	0.9414	10.6354	1.5646
8	4.24	4.8463	0.6063	6.9997	2.7597
9	5.32	4.9587	0.3613	4.1667	1.1533
10	8.81	9.2601	0.4501	10.1594	1.3494
11	8.61	8.2943	0.3157	12.1647	3.5547
12	5.55	6.0002	0.4502	3.1111	2.4389
13	13.4	12.1264	1.2736	15.8976	2.4976
14	13.1	14.1602	1.0602	16.1252	3.0252
15	3.51	3.0056	0.5044	6.9994	3.4894
16	12.2	12.9683	0.7683	8.1225	4.0775
17	6.18	5.9906	0.1894	9.9795	3.7995
18	4.49	5.1264	0.6364	7.4989	3.0089
19	4.87	4.1022	0.7678	7.6237	2.7537

20	10.21	10.9699	0.7599	7.9694	2.2406

The equation for prediction of PPV by MVRA is:

PPV = 6.406891 -0.0695 (Distance) + 0.534612 (Hole depth) -0.00465 (Charge per Hole) + 0.0346424 (Burden) + 0.673227 (Spacing) +0.056285 (No of holes)…… (5.3.1)

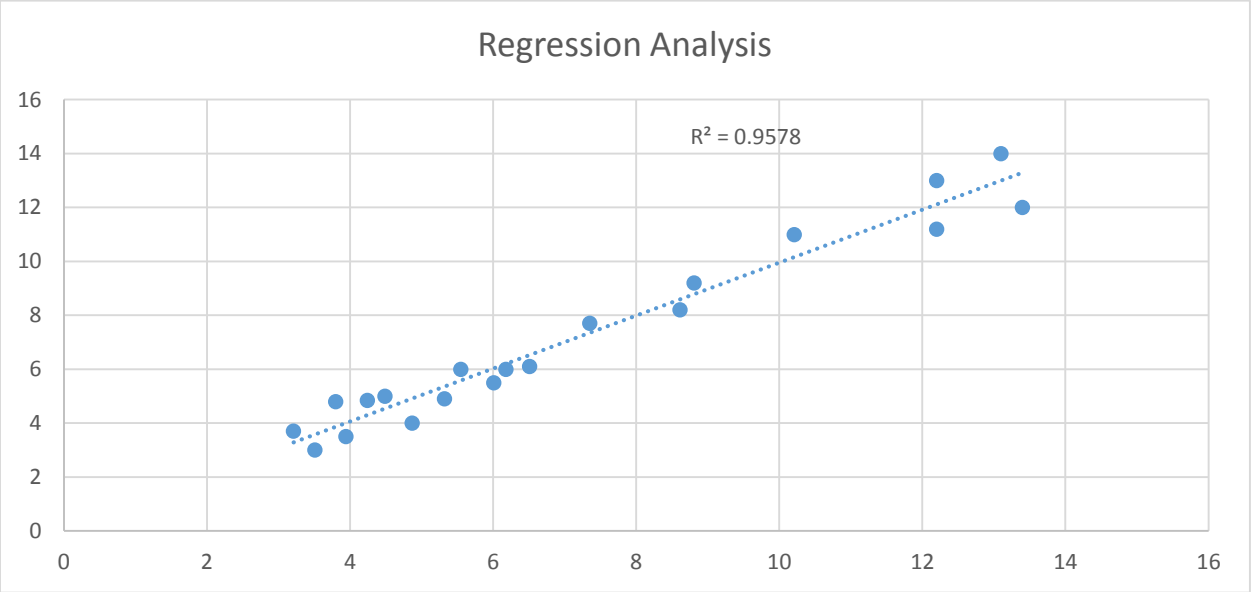

Fig 43: Regression analysis between recorded and predicted PPV of UAIL by ANN

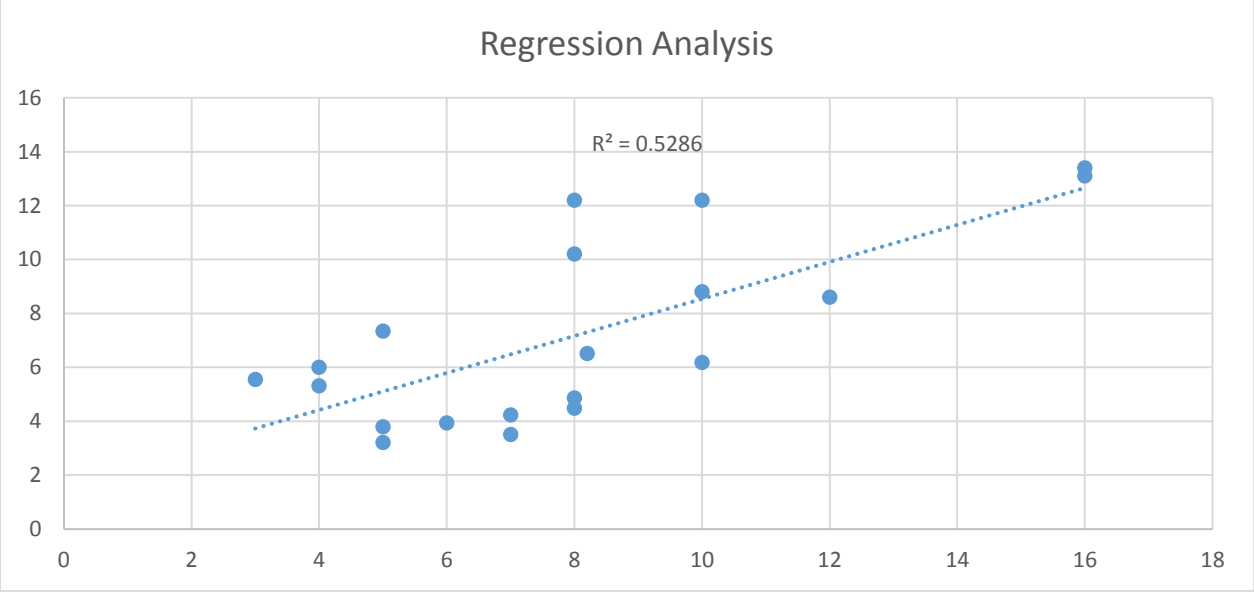

Fig 44: Regression analysis between recorded and predicted PPV of UAIL by MVRA

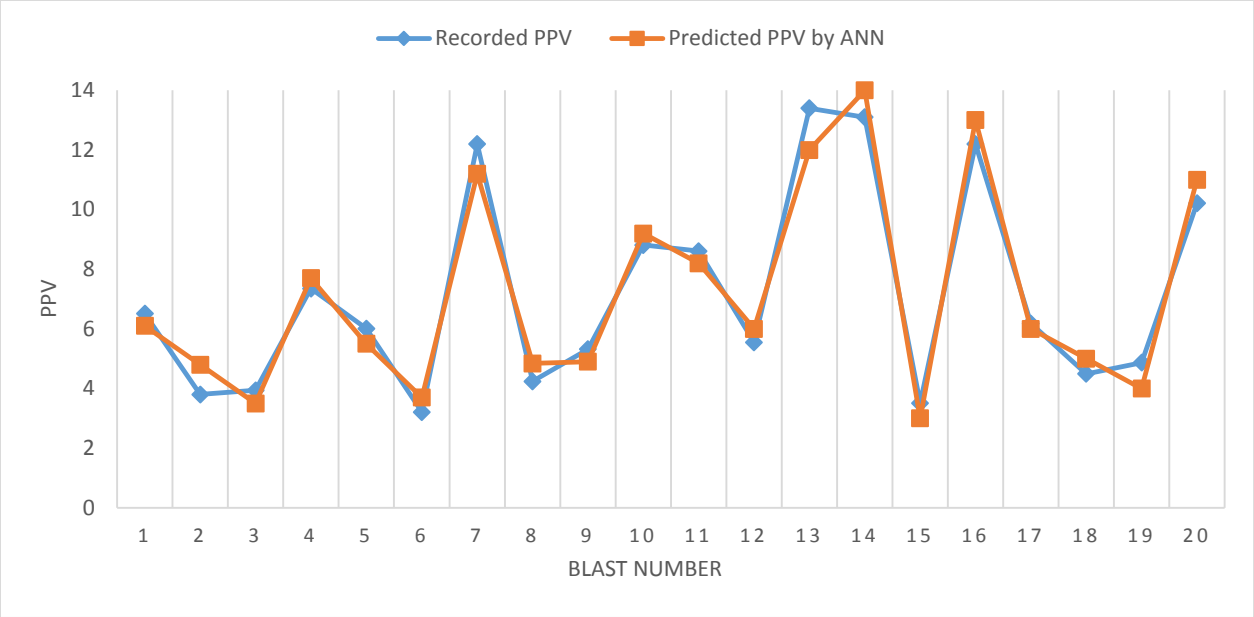

Fig 45: Line graph comparison between recorded and predicted PPV of UAIL by ANN

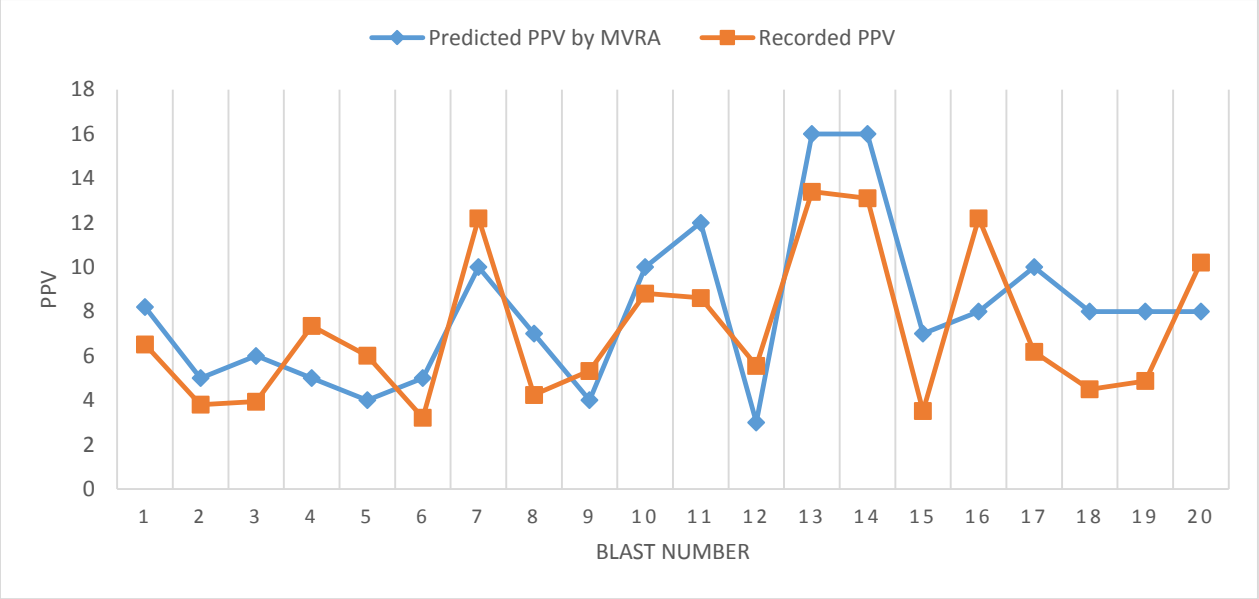

Fig 46: Line graph comparison between recorded and predicted PPV of UAIL by MVRA

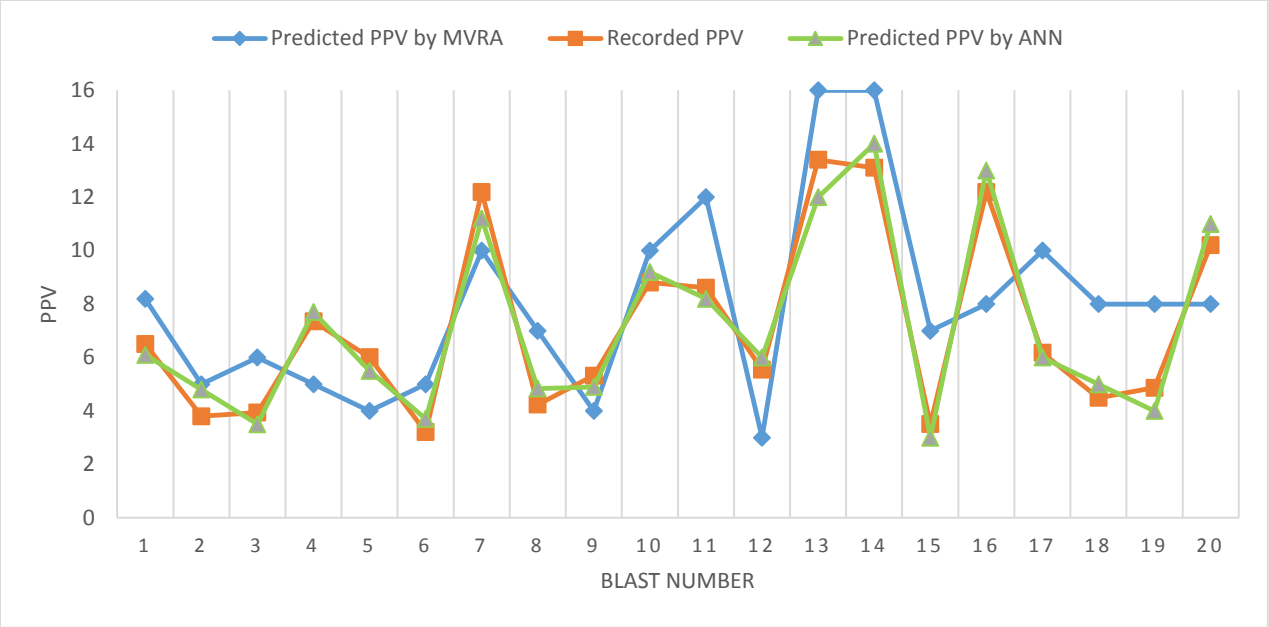

Fig 47: Line graph comparison between recorded and predicted PPV of UAIL by ANN & MVRA

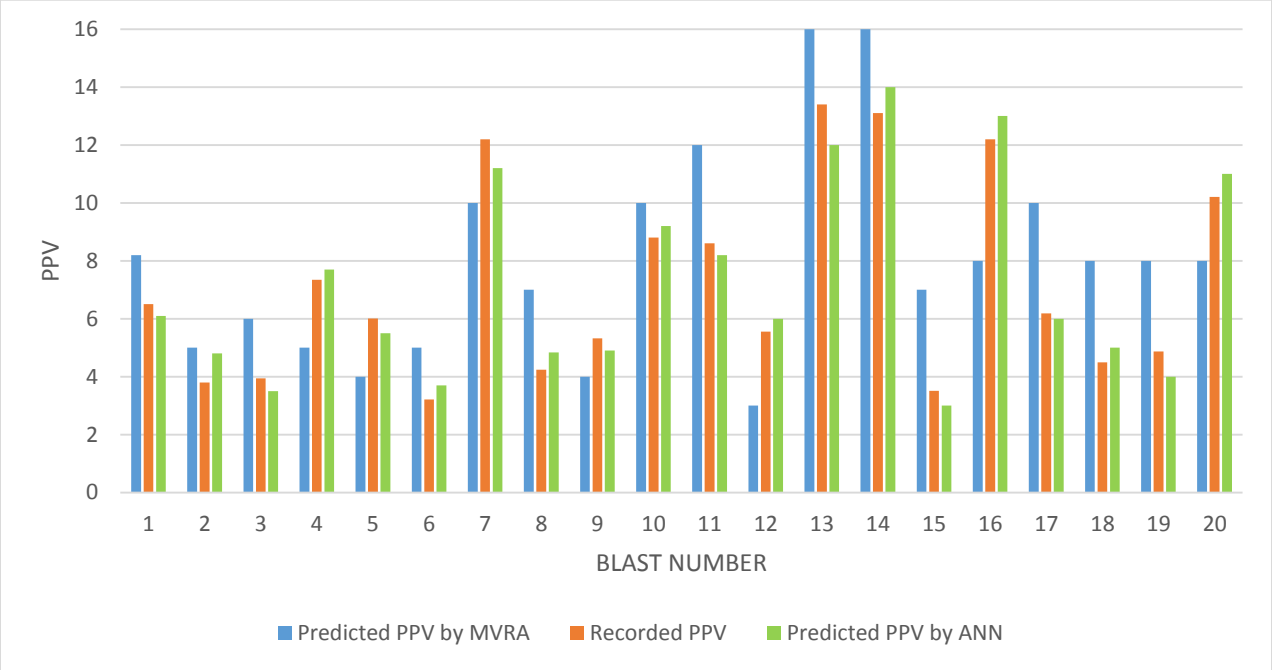

Fig 48: Bar graph comparison between recorded and predicted PPV of UAIL by ANN & MVRA

The number of input parameters taken were six for both ANN and MVRA. They were distance, hole depth, charge per hole, burden, spacing and no of holes. An error tabulation was generated between the recorded and predicted frequency. Table 12 shows the error calculation of frequency predicted by both ANN & MVRA. It shows that the error generated from prediction in ANN is lesser than the statistical analysis. The maximum and minimum error generated by ANN was 0.9607 and 0.4738 respectively whereas the maximum and minimum error generated by MVRA was 3.4503 and 1.1368 respectively. Figure 49 & 50 show the regression analysis of ANN and MVRA. The correlation coefficient determined by ANN & MVRA was 0.9721 and 0.7012 respectively. Figure 51, 52 and 53 show the line graph comparison between the recorded and predicted frequency by ANN and MVRA. Figure 54 shows the bar graph comparison between the recorded and predicted frequency by ANN and MVRA.

Table 12: Error calculation of Frequency predicted of UAIL by ANN & MVRA

Sl no.	Recorded Frequency	Predicted Frequency by ANN	Standard Deviation	Predicted Frequency by MVRA	Standard Deviation
1	12.5	11.9996	0.5004	9.9999	2.5001
2	17.7	18.4961	0.7961	21.1503	3.4503
3	4.8	4.1269	0.6731	2.2521	2.5479
4	11.3	11.9923	0.6923	13.9891	2.6891
5	12.8	12.1263	0.6737	10.1267	2.6733
6	9.9	10.5185	0.6185	11.9587	2.0587
7	8.8	8.1309	0.6691	7.1113	1.6887
8	11	11.9607	0.9607	13.1502	2.1502
9	7.5	6.9899	0.5101	6.3326	1.1674
10	6.6	7.1962	0.5962	8.0002	1.4002
11	7.1	6.2322	0.8678	5.9632	1.1368
12	6.1	6.9328	0.8328	7.9584	1.8584
13	9.5	8.9939	0.5061	8.1102	1.3898
14	12	12.9954	0.9954	13.9902	1.9902
15	7.9	7.1222	0.7778	6.2321	1.6679
16	8.6	9.1558	0.5558	10.9595	2.3595
17	11.9	11.1108	0.7892	9.1206	2.7794
18	8.6	9.1207	0.5207	10.2871	1.6871
19	7.6	7.1262	0.4738	6.100	1.4991
20	13.3	13.9652	0.6652	14.9069	1.6069

The equation for prediction of Frequency by MVRA is:

Frequency = 22.50533 - 0.01667 (Distance) + 0.641225 (Hole Depth) + 0.004224 (Charge per Hole) -4.16849 (Burden) -0.51095 (Spacing) + 0.015564 (No of holes) ……. (5.3.2)

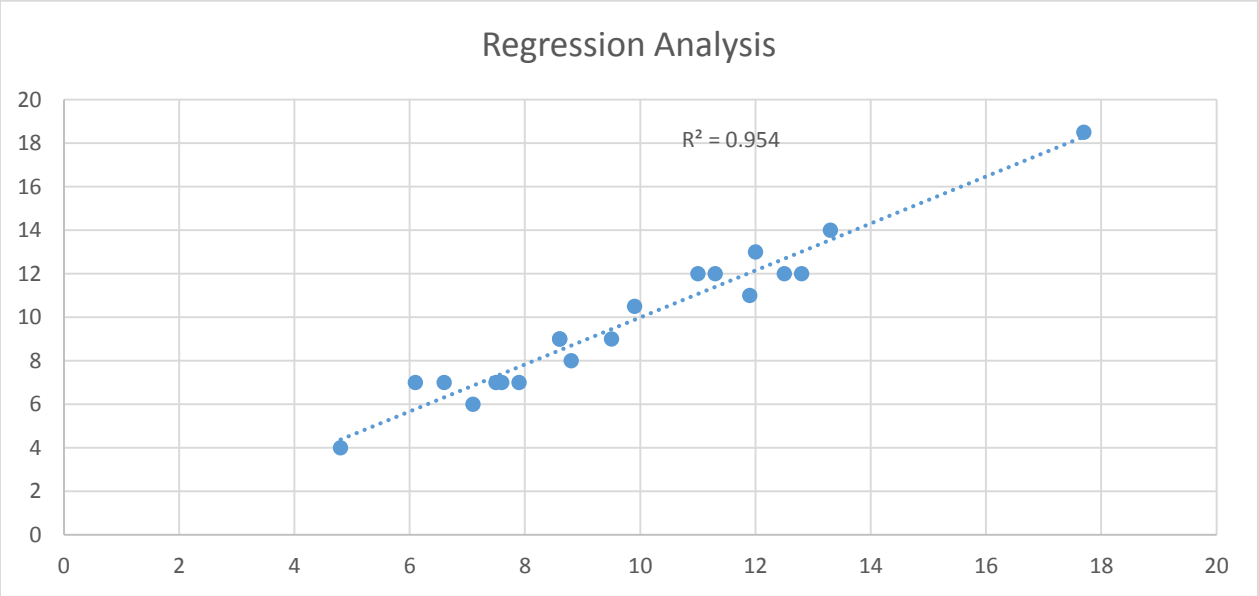

Fig 49: Regression analysis between recorded and predicted Frequency of UAIL by ANN

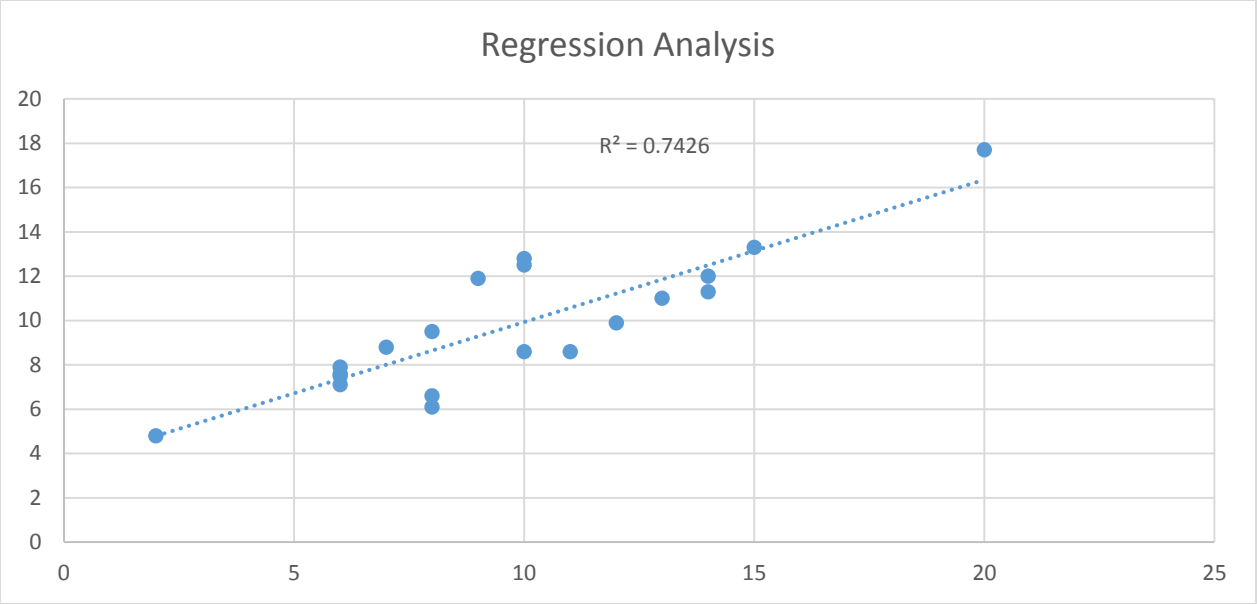

Fig 50: Regression analysis between recorded and predicted Frequency of UAIL by MVRA

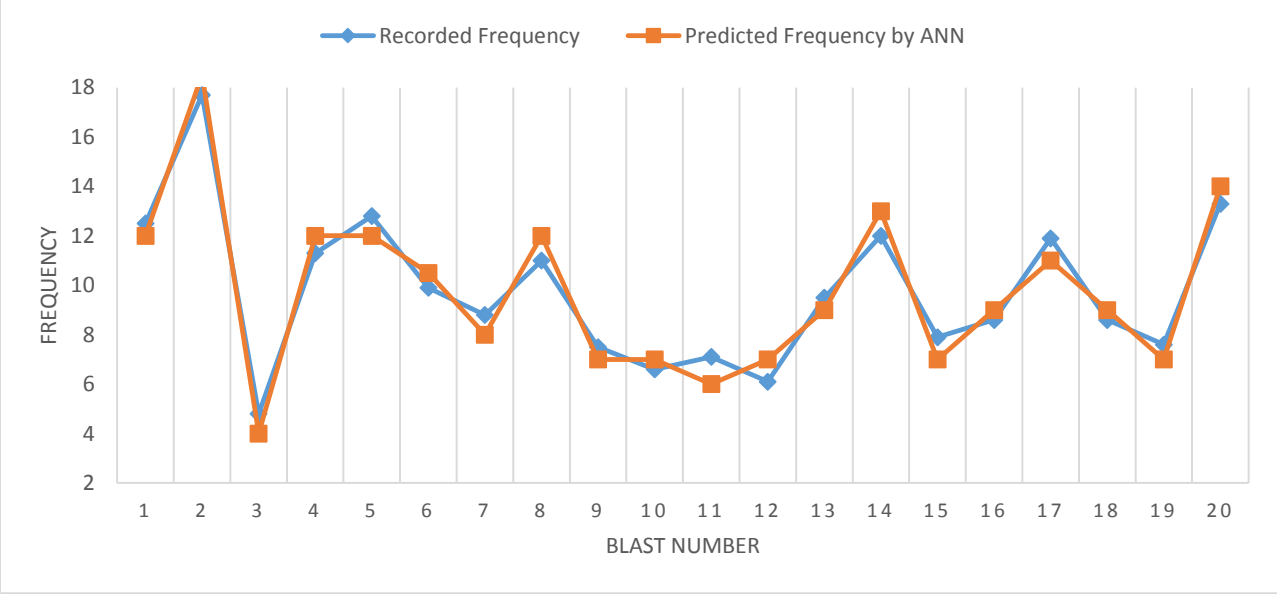

Fig 51: Line graph comparison between recorded and predicted Frequency of UAIL by ANN

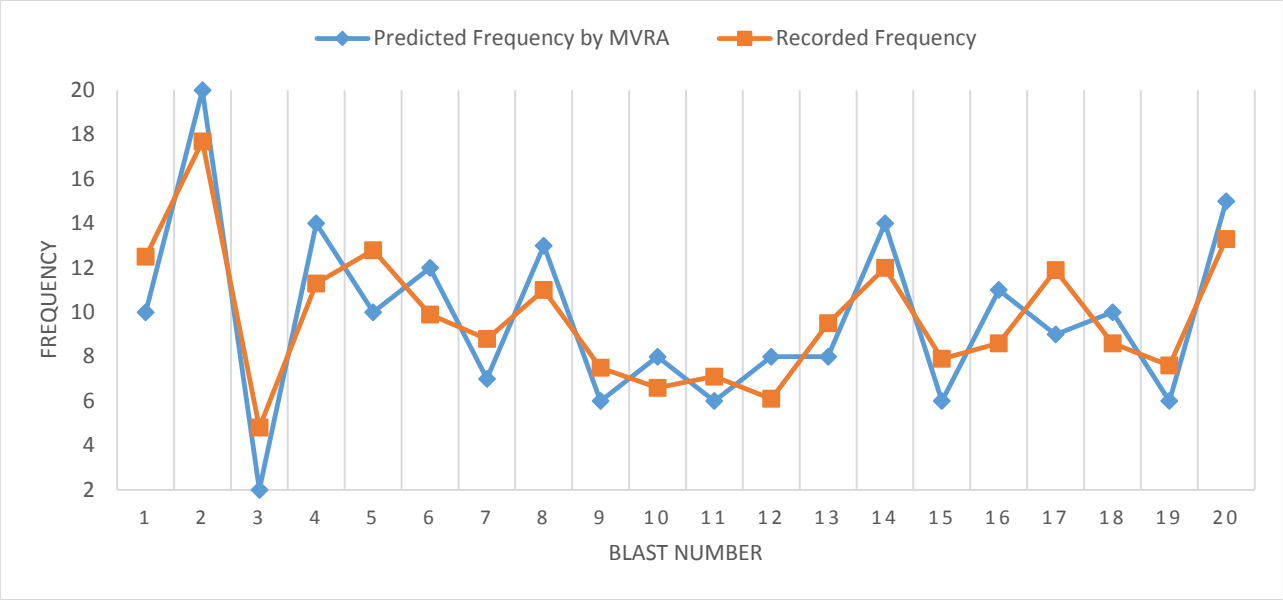

Fig 52: Line graph comparison between recorded and predicted Frequency of UAIL by MVRA

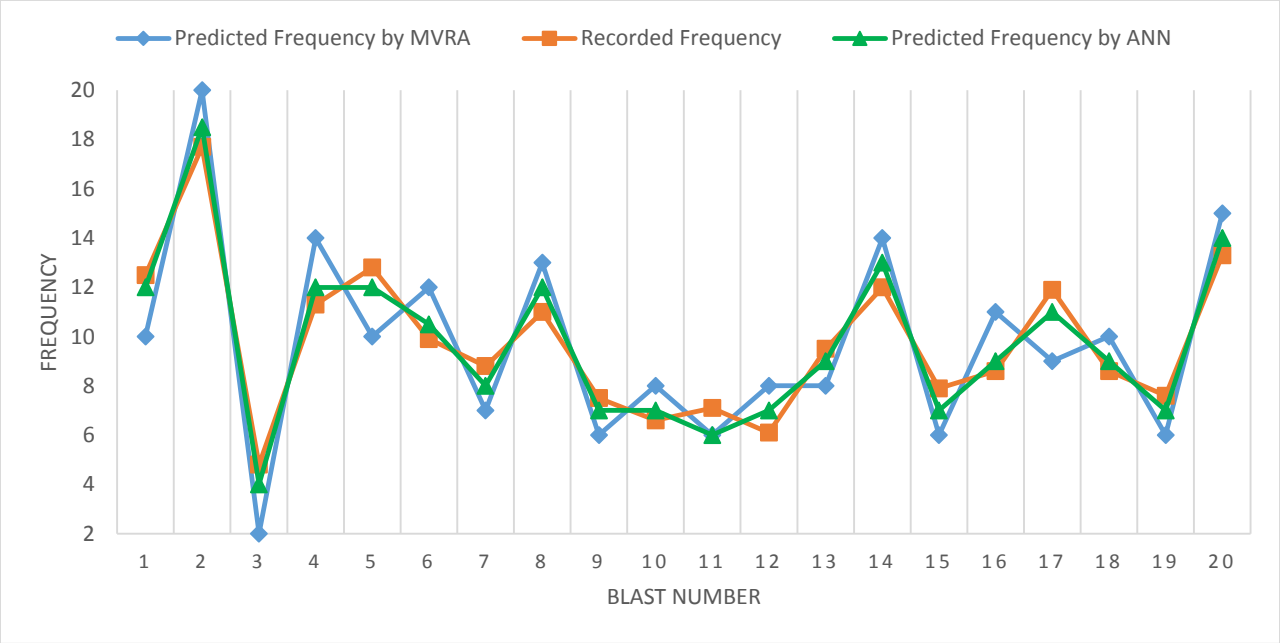

Fig 53: Line graph comparison between recorded and predicted Frequency of UAIL by ANN & MVRA

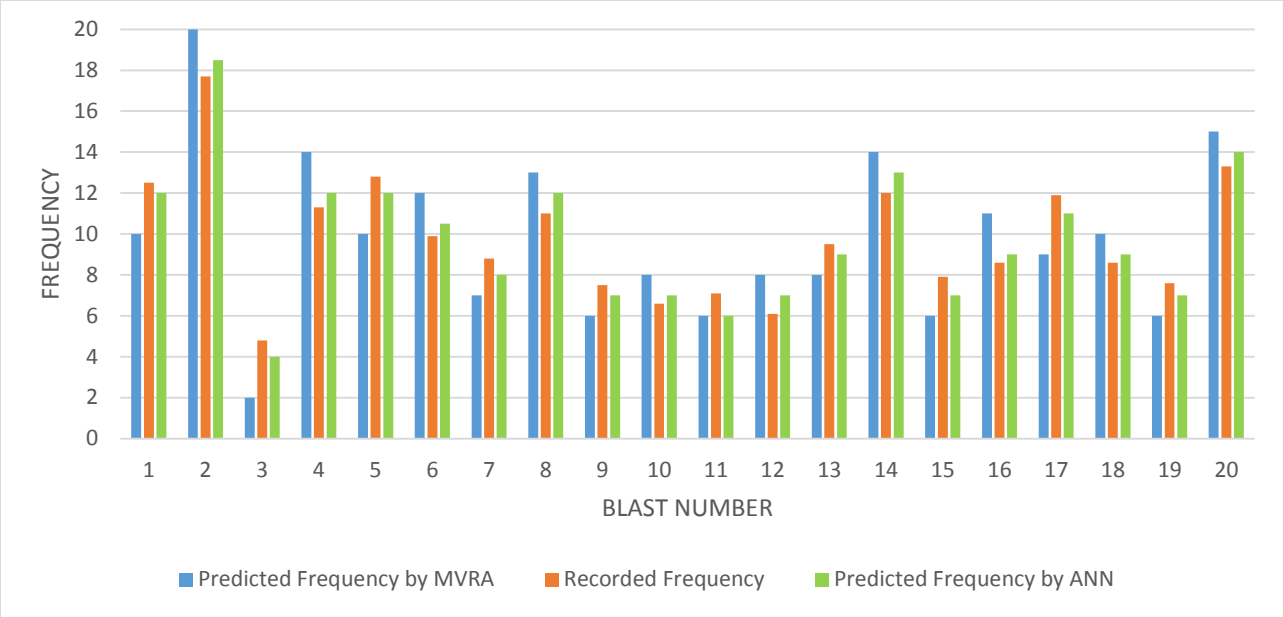

Fig 54: Bar graph comparison between recorded and predicted Frequency of UAIL by ANN & MVRA

5.4 OVERALL ANALYSIS

Table 13: Correlation coefficient between the recorded and predicted data at various mines

Name of the Mine	No. of Input Parameters	Correlation coefficient between the recorded and predicted PPV by ANN	Correlation coefficient between the recorded and predicted PPV by MVRA	Correlation coefficient between the recorded and predicted frequency by ANN	Correlation coefficient between the recorded and predicted frequency by MVRA
Dunguri Limestone mine (ACC)	06	0.9322	0.6833	0.9301	0.6667
Indian Detonators Limited Rourkela (IDL)	02	0.9053	0.5736	0.9136	0.6231
Balphimali Bauxite mine (UAIL)	06	0.9563	0.7477	0.9721	0.7012

Table 13 shows Correlation coefficient between the recorded and predicted data at various mines The correlation coefficient between recorded and predicted PPV by ANN was highest for Balphimali Bauxite mine (0.9563) and lowest for Indian Detonators Limited (0.9053). The correlation coefficient between recorded and predicted PPV by MVRA was highest for Balphimali Bauxite mine (0.0.7477) and lowest for Indian Detonators Limited (0.5736). The correlation coefficient between recorded and predicted frequency by ANN was highest for Balphimali Bauxite mine (0.9721) and lowest for Indian Detonators Limited (0.9136). The correlation coefficient between recorded and predicted frequency by MVRA was highest for Balphimali Bauxite mine (0.7012) and lowest for Indian Detonators Limited (0.6231). It shows more the number of inputs, high is the correlation coefficient.

5.5 PPV PREDICTED FOR VARIOUS MINES

DUNGURI LIMESTONE MINE, ACC

Table 14: Predicted PPV (mm/sec) by ANN at different Distances from the source of blast at ACC

Charge per hole	No of holes	Predicted PPV (mm/sec) by ANN at different Distances (m) from the source of blast (taking spacing as 4, burden as 3 and hole depth as 10)						
		At 100 m	At 200 m	At 400 m	At 600 m	At 800 m	At 1000 m	At 2000 m
30	**25**	3.53	3.01	2.55	1.67	1.24	1.02	0.56
50	**30**	4.02	3.22	2.64	1.73	1.27	1.08	0.59
40	**50**	4.11	3.41	2.68	1.78	1.33	1.12	0.61
60	**50**	4.20	3.63	2.72	1.84	1.36	1.18	0.64
80	**50**	4.44	3.73	2.78	1.88	1.42	1.23	0.67
100	**50**	4.62	3.81	2.85	1.92	1.50	1.29	0.73
200	**30**	4.86	3.89	2.91	1.95	1.60	1.33	0.77
250	**30**	4.93	4.02	2.96	1.99	1.72	1.37	0.79
250	**50**	6.21	5.11	4.01	3.04	2.82	1.42	0.81

Table 14 shows the predicted PPV by ANN at different distances from the source of blast at ACC. It suggests that at a distance of 100 m when the charge per hole is 250 kg and number of holes blasted is 50, the PPV exceeds the damage criteria of 5 mm/s. So it is safer to blast less than 30 number of holes when the charge per hole is close to 250 kg.

INDIAN DETONATORS LIMITED

Table 15: Predicted PPV (mm/sec) by ANN at different Distances from the source of blast at IDL

Weight of Explosive (kg)	Predicted PPV (mm/sec) at different Distances (m) from the source of blast						
	At 100 m	At 200 m	At 400 m	At 600 m	At 800 m	At 1000 m	At 2000 m
50.00	1.72	0.99	0.57	0.41	0.33	0.27	0.16
100.00	2.28	1.31	0.75	0.54	0.43	0.36	0.21
150.00	2.68	1.54	0.88	0.64	0.51	0.42	0.24
200.00	3.00	1.72	0.99	0.72	0.57	0.48	0.27
250.00	3.28	1.89	1.08	0.78	0.62	0.52	0.30
300.00	3.53	2.03	1.17	0.84	0.67	0.56	0.32
350.00	3.76	2.16	1.24	0.90	0.71	0.60	0.34
400.00	3.96	2.28	1.31	0.95	0.75	0.63	0.36
450.00	4.15	2.39	1.37	0.99	0.79	0.66	0.38
500.00	4.33	2.49	1.43	1.03	0.82	0.69	0.39
550.00	4.50	2.59	1.48	1.07	0.85	0.71	0.41
600.00	4.66	2.68	1.54	1.11	0.88	0.74	0.42
700.00	4.96	2.85	1.64	1.18	0.94	0.79	0.45
800.00	5.23	3.00	1.72	1.25	0.99	0.83	0.48

Table 15 shows the predicted PPV by ANN at different distances from the source of blast at IDL. It suggests that at a distance of 100 m when the charge used is 800 kg for cladding purpose, the PPV exceeds the damage criteria of 5 mm/s. So it is safer to use explosive charge of less than 800 kg for metal cladding.

BALPHIMALI BAUXITE MINE, UAIL

Table 16: Predicted PPV (mm/sec) by ANN at different Distances from the source of blast at UAIL

Charge per hole	No of holes	Predicted PPV (mm/sec) by ANN at different Distances (m) from the source of blast (taking spacing as 4.5, burden as 3.5 and hole depth as 10)						
		At 100 m	At 150 m	At 200 m	At 400 m	At 600 m	At 800 m	At 1000 m
30	**50**	2.36	2.08	1.96	1.73	1.27	1.01	0.77
40	**50**	2.97	2.32	2.26	2.22	1.38	1.21	0.87
50	**50**	3.55	2.67	2.70	2.73	1.56	1.43	0.96
60	**50**	4.37	2.97	3.11	3.21	1.92	1.67	1.13
70	**50**	5.41	3.64	3.50	3.41	2.33	1.91	1.29
80	**50**	6.77	4.13	4.09	4.02	2.71	2.29	1.41
90	**50**	7.73	5.33	5.15	4.58	3.01	2.46	1.50
100	**50**	8.61	6.13	5.77	5.44	3.52	2.83	1.67
120	**50**	9.39	7.82	6.89	6.01	4.26	3.44	1.94
150	**50**	10.41	9.66	8.44	6.53	4.99	3.91	2.21

Table 16 shows the predicted PPV by ANN at different distances from the source of blast at UAIL. It suggests that at a distance of 100 m when the charge per hole is 70 kg and number of holes blasted is 50, the PPV exceeds the damage criteria of 5 mm/s. So it is safer to blast less than 50 number of holes when the charge per hole is close to 70 kg.

CHAPTER-6
CONCLUSIONS AND SCOPE FOR FUTURE WORK

6.1 CONCLUSIONS

Based on data obtained from field work, artificial neural network analysis and multivariate regression analysis, following conclusions are made.

1) The correlation coefficient determined for PPV and frequency by ANN for Balphimali Bauxite mine (UAIL) was 0.9563 and 0.9721 respectively and correlation coefficient determined for PPV and frequency by ANN for IDL was 0.9053 and 0.9136 while correlation coefficient determined for PPV and frequency by ANN for Dunguri Limestone mine (ACC) was 0.9322 and 0.9301.
2) From ANN analysis, it was observed that more the no. of input parameters better is the correlation coefficient between the recorded and predicted data. It was also observed that when the no. of input parameters is same, the no. of testing data sets affects the correlation coefficient, more the no. of testing data sets more is the correlation coefficient.
3) ANN having better R-squared value (correlation coefficient) than conventional statistical approach, it was used to predict PPV at various distances with explosive charge values keeping other input parameters constant. Safe explosive limits were predicted for the three mine sites using artificial neural network. For UAIL the safe explosive limit was 150 kg per hole for distance of 100m. Similarly, the safe explosive limit for metal cladding at IDL at a distance of 100m was found to be 700 kg and for ACC it was 250 kg per hole for a distance of 100m.

6.2 SCOPE FOR FUTURE WORK

In this thesis study, the neural network has shown the ability to predict the peak particle velocity with a satisfactory accuracy, hence, for further study, it is recommended that other parameters affecting the ground vibrations should be designated and included in the training neural network model. Modelling of PPV and frequency can be done for different structures, buildings and storeys using softwares like STAAD and RAM.

REFERENCES

REFERENCES

1. Aimone-Martin C. T., Martell M. A., McKenna L. M., Siskind D. E., Dowding C. H., (2003) Comparative Study of Structure Response to Coal Mine Blasting. U.S. Office of Surface Mining.
2. http://www.osmre.gov/blastingindex.htm
3. Arseven B. 2003, "Blasting Optimization for the Assessment of Ground Vibrations at DemirBilek Panel of TunçBilek Mine. Msc. Thesis, the Middle East Technical University, Ankara, Turkey, pp. 12-14.
4. Dimitrios C. Kaliamparkos and Dimitrios G. Damigos, (2001) Blasting Vibration Limits to Prevent Human Annoyance Remarks from some Case Studies. Mineral Resources Engineering, Vol. 10, No. 1, pp.71-82.
5. Djordjevic N., Kavetsky A., and Scott A. Blast Design Optimization to Minimize Induced Vibrations of Structures. International Journal of Blasting and Fragmentation. (1990), pp. 373-380.
6. Esen, S. and Bilgin H. A., Evaluation of Blast Vibrations from Sekköy Surface Coal Mine in Turkey, Proceedings of the Twenty-Seventh Annual Conference on Explosives and Blasting Technique. Orlando, Florida, USA, Jan., 2001, Vol. 1, pp. 313-327.
7. Kahriman A., (2001a), Prediction of Particle Velocity Caused by Blasting for an Infrastructure Excavation Covering Granite Bedrock. Mineral Resources Engineering, Vol. 10, No. 2, pp. 205-218.
8. Kahriman A., (2001b), Analysis of Ground Vibrations Caused by Bench Blasting at Can Open-pit Lignite Mine in Turkey. Environmental Geology, Vol. 41, pp. 653-661.
9. Khandelwal M, Singh TN (2005) Prediction of blast-induced air overpressure in opencast mine. Noise Vib Worldw 36:7–16
10. Khandelwal M, Singh TN (2006) Prediction of blast-induced ground vibrations and frequency in opencast mine—a neural network approach. J Sound Vib 289:711–725
11. Khandelwal M, Singh TN (2009) Prediction of blast-induced ground vibrations using artificial neural network. Int J Rock Mech Min Sci 46:1214–1222
12. Khandelwal M, Singh TN (2002) Prediction of waste dump stability by an intelligent approach. In: National symposium on new equipment—new technology, management and safety, ENTMS, Bhubaneshwar, pp 38–45

13. Khandelwal M (2008) Evaluation and prediction of blast-induced ground vibration and frequency for surface mine—a neural network approach. Ph.D. Thesis, Indian Institute of Technology, Bombay, India
14. Maity D, Saha A (2004) Damage assessment in structure from changes in static parameters using neural networks. Sadhana 29:315–327
15. Mehrotra, K. G., Mohan, C. K., and Ranka, S. Elements of Artificial Neural Networks. MIT Press, Cambridge, 1996, pp 65-156.
16. Mohamed MT (2009) Artificial neural network for prediction and control of blasting vibrations in Assiut (Egypt) limestone quarry. Int J Rock Mech Min Sci 46:426–431
17. Monjezi M, Dehghani H (2008) Evaluation of effect of blasting pattern parameters on back break using neural networks. Int J Rock Mech Min Sci 45(8):1446–1453
18. Neaupane KM, Adhikari NR (2006) Prediction of tunneling induced ground movement with the multi-layer perceptron. Int Journal Tunnel Underground Space Technology 21:151–159
19. Nicholls, H. R., Johnson, C. F., and Duvall, W. I. Blasting Vibrations and Their Effects on Structures. BuMines Bull. 656, 1971.
20. Nick, S., Preliminary Vibration Assessment - Tahi Street, Mapua, Nelson. Report Prepared for TONKIN & TAYLOR LTD., (2002). http://www.tdc.govt.nz/pdfs/394.pdf.
21. Rumelhart, D. E., Hinton, G. R., and Williams, R. J., Learning Internal Representations by Error Propagation, in Parallel Distributed Processing, Vol. 1, D. E. Rumelhart, and J. L. McClelland, eds., MIT Press, Cambridge, MA, 1986.
22. Saha, A., A Tutorial on Neural Network Based Modeling - for beginners. http://www.geocities.com/adotsaha/index.html
23. Singh S. P., The Effects of Shock and Gas Energies on Fracturing Process. Proceedings of the 25th Annual Conference of Explosives and Blasting Technique., p397-406, Tennessee, USA, February, 1999.
24. Singh TN. A study of blast induced ground vibration at Dharapani Magnesite Mine, Pitthoragarh Himalaya, India. In: Proceedings of the third international symposium on headwater control, New Delhi; 1995. p. 183–8.
25. Tsoukalas L. H., Uhrig R. E. (1996). Fuzzy and Neural Approaches in Engineering. John Wiley Publishing Company.